

Grant Agreement No.: 318600

SODALES

SOftware-Defined Access using Low-Energy Subsystems

Funding Scheme: ***Small or medium-scale focused research project STREP - CP-FP-INFSO***
Activity: **ICT-8-1.1 - Future Networks**

D1.2 SODALES ARN Modelling

Due date of the Deliverable: Month 9

Actual submission date: 30th September 2013

Start date of project: November 1st 2012 Duration: 36 months

Project Manager: Carlos Bock | i2CAT

Version: 1.0

Author List: Michael Parker (UEssex), Carlos Bock (i2CAT), Volker Jungnickel (HHI), Victor Marques, André Brízido, Tiago Mendes (PTI), David Levi (Ethernity)

(Include as authors technical and language reviewers)

Project co-funded by the European Commission in the 7 th Framework Programme (2007-2013)		
Dissemination Level		
PU	Public	✓
PP	Restricted to other programme participants (including the Commission Services)	
RE	Restricted to a group specified by the consortium (including the Commission Services)	
CO	Confidential, only for members of the consortium (including the Commission Services)	

Abstract

This deliverable D1.2 “ARN Modelling” provides a comprehensive overview of the research technologies, methodologies and modeling results undertaken during the 1st year of the SODELES project, with respect to active remote node (ARN) design specifications. A study of advanced electro-optic and all-optical technologies that could provide the advanced ARN functionalities is provided, although the solution of the final demonstrator is anticipated to be electrical. In addition, different (electrical and optical) Ethernet topologies enabling open access networking (OAN) is discussed, as well as the implications for meshing and achieving network resilience. RF (60GHz) and optical wireless final-drop technologies interfacing the ARN and end-users are described, along with experimental results for high capacity line-of-sight (LoS) optical wireless solutions. A comprehensive and innovative theory for an absolute energy efficiency theory is described, which provides a fundamental basis for the comparative analysis of converged (wireless and wireline) communications systems, each with different noise sources to be made. A brief discussion of some of the renewable powering approaches that could provide remote and independent energy to a stand-alone ARN architecture is also provided. Finally, simulations results of a service quality analysis, for a novel flow scheduler approach optimizing the traffic bandwidth management at the ARN over two (low and high priority) wavelengths connecting the ARN to the CO for differentiated service provisioning for the various types of end-users are described.

Document Revision History

Version	Date	Description of change	Authors
1.0	30/9/2013	Final Version	M. Parker, C. Bock, V. Jungnickel, V. Marques, A. Brizido, T. Mendes, D. Levi

Table of Contents

1	Introduction	1
2	ARN Switching Technologies and Performance Assessment	3
2.1	All-optical geometries	3
2.1.1	Wavelength Converters.....	4
2.1.2	All-optical Processing	5
2.1.3	Optical Buffers/Memories	6
2.1.4	Optical Switches.....	7
2.1.5	Wavelength Filters	7
2.1.6	All-optical 2R/3R Regeneration	8
2.1.7	Discussion Remarks.....	8
2.2	Open Access Networking (OAN) Opportunities.....	8
2.2.1	Optical transport.....	11
2.2.2	Electrical-bitstream transport.....	12
2.3	Traffic Management Technologies.....	16
2.4	Meshing & Resilience	17
2.4.1	Optical resiliency	17
2.4.2	Switching resiliency	18
3	Wireless Final-Drop Technologies	19
3.1	High-Capacity 60-GHz Wireless Links	21
3.1.1	Spectral Efficiency.....	22
3.1.2	MIMO at mm-wave frequencies.....	23
3.1.3	Low-cost Components.....	24
3.1.4	Real-Time Signal Processing	24
3.1.5	Reconfigurable Radio System (RSS)	25
3.1.6	Line-of-Sight (LoS) Optical Solutions.....	27
4	Energy Efficiency.....	33
4.1	Methodology & Benchmarking	34
4.1.1	Definition of dB ϵ Absolute Energy Efficiency Metric.....	36
4.1.2	Derivation of Shannon Channel Capacity Theorem from Carnot's Law	37
4.1.3	Inclusion of FEC into Shannon Capacity Theorem	41
4.1.4	Application of Theory to Wireless & Wireline Communications Systems	44
4.2	CO-ARN Technologies	45
4.2.1	Optical Transport Network.....	45
4.3	Local v. Remote Powering	46
4.3.1	Wind and Solar.....	46
4.3.2	Fuel Cells	47
4.3.3	Pico Hydro	47
5	Service Quality Analysis	49
5.1	Overview of Higher Performance in Converged Access Networks	49
5.2	Traffic Patterns	51
5.3	Flow Scheduling for SODELES Network.....	51
5.3.1	Problem Statement	52
5.3.2	Software-Defined Networking for ARN	53
5.3.3	Topology Manager	53
5.3.4	Traffic Manager	54
5.4	Throughput Simulation Results & Discussion.....	56
6	Conclusions.....	59
7	References.....	60

List of Figures

Figure 1: All-optical ARN architecture.....	4
Figure 2: Wavelength converter block diagram [1].....	4
Figure 3: Optical networks with various signal processing functionalities. ONE: optical network element; AP: access point [4]	6
Figure 4: Schematic of all-optical variable delay buffer [7]	6
Figure 5: All-optical selective wavelength converter/data eraser for phase-modulated signals in a single SOA-MZI [11]	7
Figure 6: Schematic of an ETR filter [13]	8
Figure 7: Open Access Network (OAN) relationship model	9
Figure 8: Typical OAN topology featuring ARN functional nodes.....	10
Figure 9: Dedicated wavelength service (ARN by-pass)	11
Figure 10: Wavelength segmentation	12
Figure 11: ARN interconnections.....	12
Figure 12: E-Line service type: point-to-point	13
Figure 13: E-LAN service type: multipoint-to-multipoint	14
Figure 14: E-Tree with hub-and-spoke multipoint connectivity	14
Figure 15: Optical mesh topology	17
Figure 16: OADM resilient topology	17
Figure 17: Electrical mesh topology.....	18
Figure 18: Cache-and-forward network architectures featuring high-capacity wireless networks [15]	19
Figure 19: RF technology application scenarios into 2015 and beyond (adapted from [15]).	20
Figure 20: 60 GHz 1GbE backhaul link [27]......	21
Figure 21: 24 GHz, 1GbE backhaul link [28].....	21
Figure 22: DSQ-128 Modulation.....	22
Figure 23: Singular values of MIMO modes versus the inter-element spacing in 70 GHz mm-wave link after 1 km distance. Left: 2x2 MIMO with linear arrays at both sides. Centre: 4x4 MIMO with linear arrays. Right: 2x2 LOS-MIMO from [40].....	23
Figure 24 (a) & (b): Examples of 60-90 Hz mixer chips [40].....	24
Figure 25: Schematic 60 GHz GbE real-time wireless system [41]	25
Figure 26: Key functional elements associated with reconfigurable radio systems [42].....	26
Figure 27: Left: A commercial line-of-sight link [24]. Right: Bidirectional optical wireless links based on LEDs, originally developed for indoor applications. For further information, see www.hhi.de.....	27
Figure 28: WDM principle for VLC showing in-parallel transmission of three (RGB) channels and reception of one channel via color filtering.....	30
Figure 29: The overall bidirectional real-time line-of-sight (LOS) VLC link.	30
Figure 30: Real-time 500 Mb/s VLC system, as shown at a commercial exhibition (right) with the zoom-in of the desk part (bottom left) and the long-range (up to 20 m) version (top left).	31
Figure 31: Measurement results for the real-time VLC system. Left: Achieved data rates for the red LED-based transmitter depending on the light intensity measured using a standard photometer at the receiver entity. Right: Measured bidirectional data rates over varying transmission distances demonstrating the virtually colour-independent data transmission.	32
Figure 32: Left: Traditional PON architecture. Right: In an actively switched architecture, the passive node and amplifier is replaced by an ARN in the first aggregation step which is also responsible for the statistical multiplexing.....	34
Figure 33: (a) Schematic diagram of a classical thermodynamic heat engine; (b) Equivalent representation showing the entropy states of the reservoirs and the entropy flows.....	37

Figure 34: (a) Schematic diagram of entropy flows for an information processor; (b) Equivalent diagram for a Shannon communications system, with channel capacity $C=dI/dt$, and associated (negative) entropy gradient $-dH/dx$	39
Figure 35: Schematic diagram of an information transmission channel with additive white Gaussian noise (AWGN), characterised using Carnot's law to derive Shannon channel capacity theorem.....	42
Figure 36: Wind and solar power generation equipment.....	46
Figure 37: Fuel cell generation experiment.....	47
Figure 38: Pico Hydro power generation systems.....	48
Figure 39: Demonstrating the user and resource interactions in point-to-multipoint access network	51
Figure 40: SODES access network architecture.....	52
Figure 41: Mapping packet flow headers to optical flow headers	53
Figure 42: Result showing the effect of flow selection techniques on throughput.....	57
Figure 43: Comparing the effectiveness of adopting a connectivity traffic measure with simple random assignment. Configuration delay is measured in seconds (s)	57

List of Tables

Table 1: Noise temperature Technology co-efficient factors	44
--	----

List of Acronyms

3GPP	Third Generation Partnership Project
AAI	Authentication, Authorisation, and Identification
ADSL	Asymmetric Digital Subscriber Line
ADSL2	Asymmetric Digital Subscriber Line and Annex J
AGP	Aggregation Point
aGW	Advanced Gateway
APON	ATM-PON
ARN	Active Remote Node
ARPU	Average Revenue Per User
ATM	Asynchronous Transfer Mode
BBU	Baseband Unit
BoF	Broadband over Fibre
BPON	Broadband PON
BS	Base Station
BTS	Base Transceiver Station
CAPEX	Capital Expenditure
CATV	Cable Television
CCM	Continuity Check Message
CDMA	Code Division Multiple Access
CFM	Connectivity Fault Management
CFP	C Form-factor Pluggable
CO	Central Office
CoMP	Co-ordinated Multi-Point
CoS	Class of Service
CPE	Customer Premises Equipment
CPRI	Common Public Radio Interface
CSI	Channel State Information
C-VLAN	Customer VLAN
DBA	Dynamic Bandwidth Allocation
DSL	Digital Subscriber Line
E2E	End-to-End
EFM	Ethernet First Mile
Eos	Ethernet over SDH
EPON	Ethernet PON
EVC	Ethernet Virtual Channel/Connection
FDD	Frequency Division Duplex
FSAN	Full Service Access Network
FTTB	Fibre-To-The-Building
FTTC	Fibre-To-The-Curb
FTTCab	Fibre-To-The-Cabinet
FTTH	Fibre-To-The-Home
FTTx	Fibre-To-The-x
GEM	GPON Encapsulation Method
GFP	Generic Framing Procedure
GPON	Gigabit-PON
GSM	Global System for Mobile
HDTV	High Definition Television

HO	High Order
HQoS	Hierarchical QoS
HSPA	High Speed Packet Access
HW	Hardware
ICI	Inter-Cell Interference
ID	Identifier
IEEE	Institute of Electrical & Electronic Engineers
IETF	Internet Engineering Task Force
iid	independent & identically distributed
IoF	Intermediate frequencies over Fibre
IP	Internet Protocol
IPTV	IP Television
IRN	Intermediate RN
ISP	Internet Service Provider
ITU	International Telecommunications Union
JD	Joint Detection
JT	Joint Transmission
LAN	Local Area Network
LCAS	Link Capacity Adjustment Scheme
LO	Low Order
LoS	Line of Sight
LTE	Long Term Evolution
MAC	Medium Access Control
MEF	Metro Ethernet Forum
MEP	Maintenance End Point
MIMO	Multiple-Input Multiple-Output
MPLS	Multi-Protocol Label Switching
NGPON	Next-Generation PON
NNI	Network Node Interface
O&M	Operations and Maintenance
OAM	Operations, Administration and Maintenance
OBSAI	Open Base Station Architecture Initiative
ODN	Optical Distribution Network
OFDM	Orthogonal Frequency Division Multiplexing
OLT	Optical Line Termination
OMCI	ONT Management and Control Interface
ONT	Optical Network Termination
ONU	Optical Network Unit
OPEX	Operational Expenditure
ORI	Open Radio equipment Interface
P2MP	Point-to-Multi-Point
P2P	Point-to-Point
PB	Provider Bridge
PBB	Provider Backbone Bridge
PDH	Plesiochronous Digital Hierarchy
PHY	Physical layer
PON	Passive Optical Network
POTS	Plain Old Telephone Service
PPB	Parts Per Billion
PTN	Packet Transmission Network
PTP	Precision Time Protocol

PWE	Pseudo Wire Emulation
QoS	Quality of Service
RAN	Radio Access Network
RBS	Radio Base Station
RF	Radio Frequency
RF	Radio Frontend
RN	Remote Node
ROADM	Reconfigurable Optical Add/Drop Multiplexer
RoF	Radio over Fibre
RRH	Remote Radio Head
RSP	Retail Service Provider
RT	Remote Terminal
SCN	Signalling Communication Network
SDR	Software Defined Radio
SME	Small- to Medium-sized Enterprise
SNMP	Simple Network Management Protocol
SoC	System-on-a-Chip
SODELES	SOftware-Defined Access using Low-Energy Subsystems
SOHO	Small Office/Home Office
SONET/SDH	Synchronous Optical Network/Synchronous Digital Hierarchy
SP	Service Provider
SSM	Synchronous State Message
STM	Synchronous Transfer Mode
S-VLAN	Service VLAN
SW	Software
TCO	Total Cost of Ownership
TDD	Time Division Duplex
TDM-PON	Time-Division-Multiplexing PON
TD-SCDMA	Time Division Synchronous Code-Division Multiple-Access
TE	Traffic Engineering
Top	Time over Packet
TWDM-PON	TDM/WDM-PON
UDWDM	Ultra-Dense WDM
UE	User Equipment
UMTS	Universal Mobile Telecommunications System
UNI	User Network Interface
VCAT	Virtual Concatenation
VDSL	Very-high-data-rate DSL
VLAN	Virtual LAN
VoD	Video on Demand
VoIP	Voice over IP
WAN	Wide Area Network
WCDMA	Wideband Code Division Multiple Access
WDM	Wavelength Division Multiplexing
WiMAX	Worldwide Interoperability for Microwave Access
XG-PON	10-Gb/s capable PON
ZF	Zero Forcing

1 Introduction

In this deliverable D1.2 “ARN Modelling” of the SODALES project, we describe the initial results of the technical studies that have been conducted during this first year of the SODALES project into Active Remote Node (ARN) technologies. This deliverable D1.2 follows from the earlier deliverable D1.1 “SODALES Architecture, Service Catalogue, and Network Specifications”, which provided the broad outline parameters for the SODALES architecture, in particular (in the context of this deliverable D1.2) the dimensioning parameters of the ARN. We have taken these preliminary dimensioning specifications for the ARN to undertake performance modelling, to quantitatively confirm the appropriateness of the dimensioning parameters supplied from the earlier deliverable.

We have considered the potential physical configurations of the ARN, including the use of electro-optical and all-optical geometries, and the possible wireless (RF and optical) final-drop technologies suitable to connect the ARN to end-users. The different topological configurations (including meshing and resilience) for electrical or optical bitstreaming in the Open Access (OA) context are also presented. Relating to the important low-energy consumption aspects of the SODALES architecture, we also provide an innovative analysis of the fundamental energy efficiency considerations underpinning the converged SODALES access network. We briefly consider alternative, renewable energy approaches that may be employed to power the remote ARN node. Finally we provide a comprehensive service quality analysis of the traffic patterns expected to pass through the ARN. In particular, we model a flow-scheduling algorithm, suitable for the SODALES ARN, which also enables Software-Defined Networking (SDN) configurations of the ARN, to optimise capacity throughput and resource utilisation, while offering differentiated service provisioning and optimised statistical multiplexing capabilities.

The deliverable is organised as follows:

Subsequent to this Chapter 1 Introduction, we present in Chapter 2 an assessment of the available ARN switching technologies, including a discussion of the relative merits of electro-optical and high-speed all-optical ARN technologies, the impact of Open Access Networking (OAN) on the design of the electro-optic bitstream capabilities, and the different virtual Ethernet topologies required to underpin the OA requirements.

Chapter 3 discusses in detail the various wireless (RF and optical) final-drop technologies that we are expecting to exploit for the interface between end-user and ARN (in addition to the fixed-line, fibre-to-the-premises option). In particular, we highlight the multi-Gb/s capabilities possible from a 60-GHz RF infrastructure, and also the upcoming Line-of-Sight (LoS) optical solutions that are now becoming available, with recent experimental performance results reported.

Energy efficiency is considered at length in Chapter 4, where we present a novel fundamental approach to measuring the absolute energy efficiency of converged (heterogeneous) access networks. In particular, we provide the first-ever thermodynamic approach using the Carnot Law to derive the Shannon channel capacity theorem, with a powerful tool to incorporate any noise model (e.g. additive white Gaussian noise, or impulsive noise) into the energy efficiency considerations. With wireless and fibre-optic communications systems possessing very different noise properties, such a common approach will provide an important tool for the comparative analysis of a converged access network infrastructure. An overview of low carbon footprint, local powering solutions, exploiting various renewable energy sources is also presented, all of which are suited to providing the relatively modest powering requirement of the SODALES ARN.

In chapter 5, we describe some initial simulation results of the expected service quality exhibited by the ARN. In particular, a time-series user traffic statistics model provides the input to a management function (designed using SDN principles) to dynamically allocate traffic over two wavelengths between the ARN and the Central Office (CO). Particular attention has been paid to considering the requirements for a converged (integrated) wireless-wireline ARN traffic profile. Preliminary results indicate that a 20% increase in data traffic throughput, with a 40% reduction in time delay (latency) is possible using our novel flow scheduler approach.

Finally, in chapter 6, we present some concluding remarks.

2 ARN Switching Technologies and Performance Assessment

In this chapter, we present an overview of the different electro-optic and all-optical technologies currently available to provide the advanced SODELES switching functionalities required at the active remote node (ARN). Most of these technologies are still only at the research stage and are not expected to start appearing in commercial telecommunications systems for some years (e.g. in the core or optical transport networks), yet alone appearing in the highly cost-sensitive and physically-demanding environment that is represented by access networks. However, we include this analysis to provide an overview of what may be possible in the future, as viable technological solutions for ever-increasing bandwidths (in accordance with Nielsen's law) and higher access speeds. In the relatively short-term timeframe of the SODELES project, we expect that electronic technical solutions will still offer the most effective cost-benefit analysis for incorporation in the ARN node architecture. However, in designing the final ARN demonstrator for the SODELES project, we will be aiming to allow for future-proofing and upgrading possibilities using these more advanced technical solutions.

We also consider the different ARN topologies that will enable the most effective (and again, future-proofed) open access networking potentialities. In particular, in this chapter we discuss the possibilities for both electrical and optical bitstreaming transport capabilities. Allied to this, we also introduce our basic approach to traffic management in the ARN (discussed at greater length in the accompanying deliverable D1.3) and the associated technologies to enable network resilience in the SODELES access architecture.

2.1 All-optical geometries

The architecture of an all-optical ARN solution is indicated in Figure 1, which is based on utilization of well-understood and available devices, but many of which will still need the specific design and fabrication of custom-design components to allow optimal SODELES functionality. Instead, during the course of this project, our motivation is to design a practical, commercially viable ARN device with a robust and cost-effective solution within a feasible timeframe. However, the architecture of Figure 1 contains a set of important functionalities and optical components, which we consider at greater length in the following sections, so as to provide an insight into possibilities for future optical switching capability in the ARN.

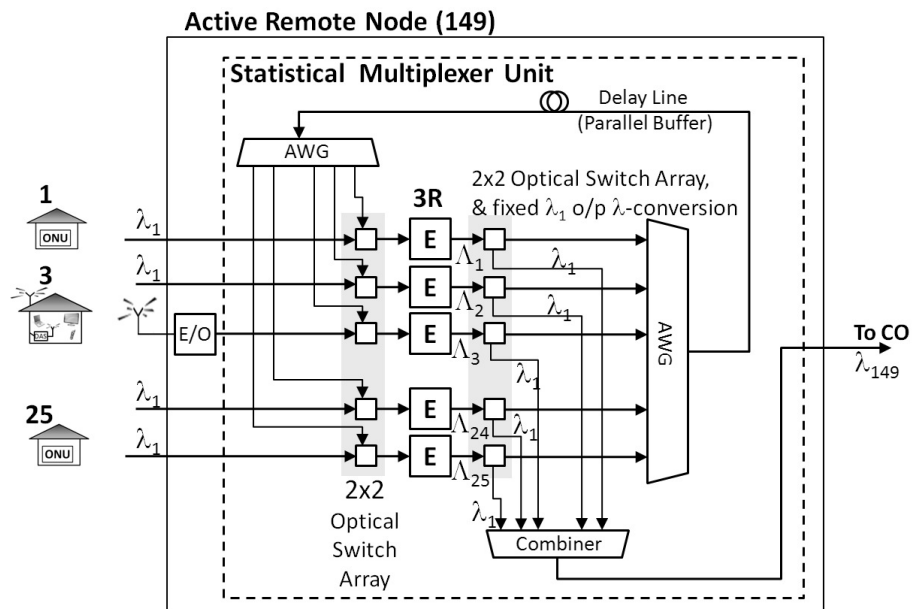


Figure 1: All-optical ARN architecture

2.1.1 Wavelength Converters

Networks efficiency can be improved by utilizing wavelength converters in WDM networks. A common problem in an optical network is the wavelength-continuity constraints where all the links in the network path are required to have allocation of the same wavelength to establish a lightpath. The wavelength-routed network can be distinguished from a circuit-switched network, which the former method accepts no connection when the capacity along any of the links in the path has reached to its limit. A wavelength converter functions in a manner where data can be converted from an input wavelength onto a different output wavelength among the N wavelength in the system (Figure 2). In Figure 2, the input signal wavelength, the converted wavelength, and the pump wavelength are characterised by λ_s , λ_c , and λ_p , respectively [1].

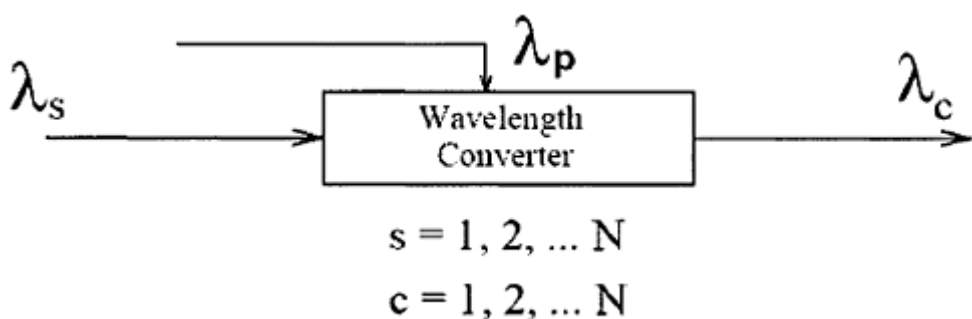


Figure 2: Wavelength converter block diagram [1]

The range of wavelengths that can be handled at the inputs and outputs can classify the wavelength converters where the configuration is a fixed-input/fixed-output or/and a variable-input/variable-output. Additionally, it is required to consider the operating range of input optical powers, the input signals transparency with regard to the bit rate and modulation format, and the possible forming of additional noise and phase jitter to the signal. The polarization-dependent

loss should be kept to minimum for all-optical wavelength converters. Wavelength conversion can be achieved in four fundamental technologies: optoelectronic, optical grating, interferometric, and wave mixing. All-optical converters can be achieved from the latter three methods [1].

An experiment has been demonstrated for transparent all-optical WDM wavelength multicast in [2] to confirm the application of Multi-Wavelength Conversion (MWC) by cross-phase modulation (XPM) in a semiconductor optical amplifiers-based Mach-Zehnder interferometer (SOA-MZI). It is suggested that higher bit rate such as 40-Gb/s application can be used for MWC through a faster SOA dynamics. All-optical wavelength conversion to demonstrate 160 Gb/s rate is presented in [3] utilizing a single SOA where 0.5 W of electrical power is required to operate and the power penalty is <3 dB.

The ARN architecture in SODELES will benefit greatly from the all-optical wavelength converters in order to improve the network efficiency with regard to increased routing capacity in addition to improved flexibility in the network functionality.

2.1.2 All-optical Processing

In the past decade, the Internet traffic has been increasing exponentially. Undoubtedly the growth will continue to accommodate considerable distances covered in fibre optics, optical communication systems and networks. At present, operation of optical links at 10-Gbit/s or 40-Gbit/s is developed and links with 100-Gbit/s and 400-Gbit/s links are under development. The transmission capacity limits are constantly being pushed by researches in order to meet the ever-growing bandwidth requirements [4]. The existence of ultrafast nonlinear optical phenomena has caused the design of photonic nodes operating at the Tbit/s line rates to be enabled by optical signal processing without the requirement for extensive optical-electrical-optical (OEO) conversions [5, 6].

Optical signal processing has many advantages such as reduction in network latency and increased efficiency, especially for many division-multiplexed channels (e.g. SDN, WDM and PDM) while offering data rates greater than 100-Gbit/s. Furthermore, optical signal processing benefits from transparency and scalability [4]. Components and subsystems of an optical signal processing, such as optical network elements (ONEs) and access points (APs), can be located in various sections of an optical network as illustrated in Figure 3.

The employment of all-optical signal processing can produce practical challenges for ultrahigh speed optical systems and networks, such as bit-rate scalability, buffering competence, and transparency to modulation formats and to network traffic [4]. Considering the SODELES ARN architecture, all-optical processing can improve data rates and efficiency in various devices in the ARN thus, network latency will be reduced.

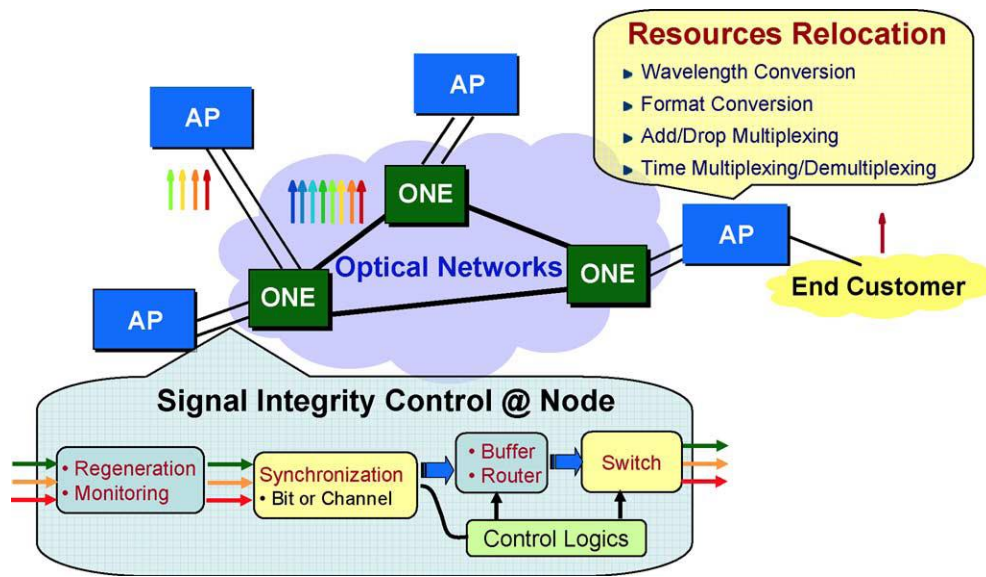


Figure 3: Optical networks with various signal processing functionalities. ONE: optical network element; AP: access point [4]

2.1.3 Optical Buffers/Memories

One of the advantages of an all-optical network is the increased capacity. The capacity growth can be limited by technical problems such as packet contention, when two or more incoming packets, with the same wavelength, compete for the same output at the same time. Packet contention occurs more frequently in asynchronous and variable-sized packet switching than synchronous and fixed-size packet switching. Utilization of fibre Bragg gratings (FBGs) to design an all-optical variable delay buffer can offer variable delay times while the contenting packets can be stored for a relatively long time. In this method (as shown in Figure 4), a simple architecture is employed to extract the delayed packets as soon as the control unit makes a decision. The advantage of this design, in addition to the variable delay times, is its all-fibre geometry, low insertion loss, and low cost prospective. In a scenario where 16 wavelengths are used in an optical network, it was found that the contenting packets can be delayed up to 169.2 μ s [7].

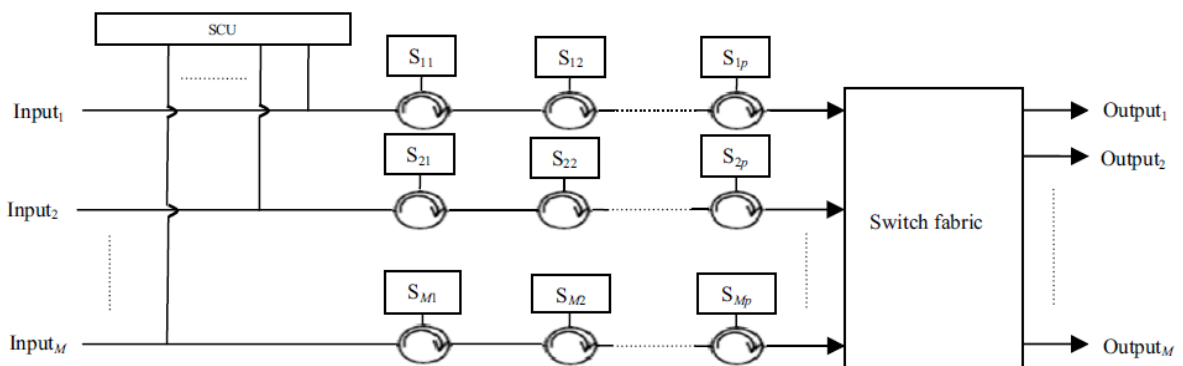


Figure 4: Schematic of all-optical variable delay buffer [7]

A SOA-based all-optical buffering technique can be used in a re-circulating fibre loop with phase-modulated signals, such as DQPSK. The packet payload rate does not have an effect in this scheme and a maximum delay of 25 μ s can be reached while storing data packets for ten rounds. Crosstalk measurements demonstrate the suitability of this buffer in all-optical networks [8, 9].

The SODALES architecture will significantly benefit from the utilization of optical buffering as variable delay time can enhance the performance of contention packets to achieve a further delay in addition to all-fibre geometry characteristics and low insertion loss.

2.1.4 Optical Switches

An optical-to-electronic-to-optical (OEO) conversion is required in the current networking equipment in order to convert optical signals to electrical ones so that they can be amplified, regenerated or switched, and then reconverted back to optical signals. The capacity bottleneck caused by electronic switching can be avoided in optical networks utilizing the all-optical switching fabrics. The absence of OEO conversion is the characteristic of all-optical switch networks [10].

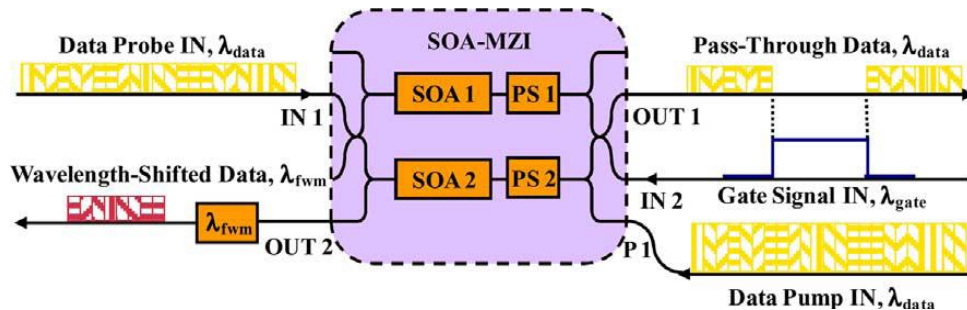


Figure 5: All-optical selective wavelength converter/data eraser for phase-modulated signals in a single SOA-MZI [11]

For next-generation high-capacity optical networks, the most sustainable solution is the coherent optical systems. An all-optical selective switching utilizing a single semiconductor optical amplifier Mach-Zehnder interferometer (SOA-MZI) can be employed to simultaneously convert the data wavelength in the original signal. In this method, a flexible network can be enabled in multichannel coherent systems by dynamic wavelength routing and add/drop operation [11]. The utilization of optical switches provide beneficial advantages in the SODALES architecture since fast switching time offers an operation of up to 40 Gb/s data rate [12]. Furthermore, the semiconductor-based technology suggests a suitable scheme for photonic integration and reduced operating power and footprint [11].

2.1.5 Wavelength Filters

A two-dimensional (2D) finite-difference time-domain (FDTD) can be used to design an equilateral triangle resonator (ETR) filter with a directional output waveguide in order to improve device performances with regard to high output efficiency. An improvement on Q factor, finesse, extinction ratio, and intensity ratio of the transmissions on-resonance at the drop port to the through port can be made from a deformed ETR filter [13]. Diffraction efficiency can also be improved in all-optical tuneable holographic wavelength filters by optimizing the intensity ratio of the writing beams [14]. A practical fibre Bragg grating (FBG) filters can demonstrate the wavelength-offset optical filtering to improve the system optical power budget (OPB) by 1.4 dB. It suggests that utilizing of FBG filters with steep intensity response edges can improve optical systems [15].

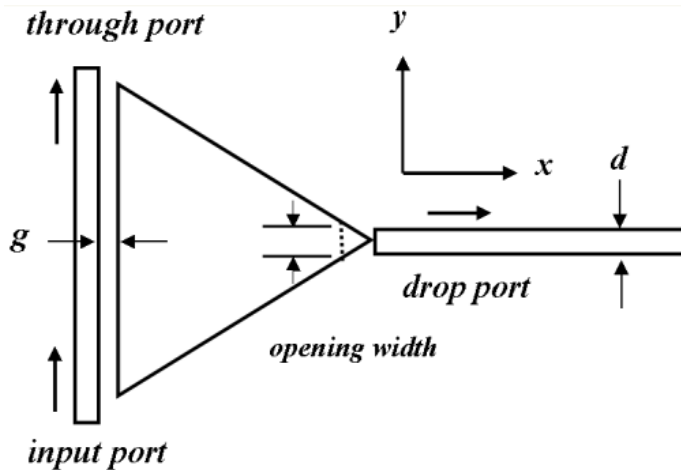


Figure 6: Schematic of an ETR filter [13]

2.1.6 All-optical 2R/3R Regeneration

As is the case for the ARN architecture in SODELES project, all-optical regeneration can facilitate the future all-optical networks with increasing demands on traffic capacity since the network configuration may be simplified without complex and bit-rate dependent optical-electrical-optical (OEO) conversion [16]. Different methods are utilized to implement all-optical signal regeneration: semiconductor optical amplifiers (SOAs) based on cross-gain-compression (XGC) [17] to obtain up to 80 Gb/s regenerative amplification; pulse trapping [18] technique to generate a gain of considerable 20 dB which is demonstrated in a 140 m-long standard low birefringence fibre; and fibre optical parametric amplifiers (FOPAs) [19] used to improve receiver sensitivity of a damaged signal by up to 3 dB. In addition, cross phase modulation (XPM) in SOA [20] can be used in an all-optical QPSK signal regeneration with a 2.3 dB power penalty. The all-optical 3R (or 2R) regeneration devices in ARN architecture of SODELES can provide power efficiency and simple integration onto the optical network.

2.1.7 Discussion Remarks

There are a number of benefits to be gained from all-optical geometries in the ARN architecture, as already outlined, but which can also include the higher network efficiency with increased user connectivity, future proofing, and potentially lower energy operation. However, the disadvantages include the decreased operating range so that the subscribers are required to be distributed in a closer proximity to the central office, and more critically the additional cost (both Capex, as well as OpEx due to reliability issues) of what are still relatively immature technologies. Overall, at this stage of the project, the intention is to realistically use electronic technical solutions to provide the SODELES functionalities in the ARN architecture; however, breakthroughs in the optical solutions described above may still offer opportunities for incorporation into the final demonstrator product.

2.2 Open Access Networking (OAN) Opportunities

Open Access Networking (OAN) is emerging as an important solution to reduce overall access network investment costs and also reduce maintenance and operations. SODELES is fully committed to provide support to Open Access standards, and more specifically, to allow fully

compatibility with bitstream Open Access, as this is the most cost-effective way to share telecom networks.

The new horizontal network architecture leads to a re-structuring of the traditional telecommunications business model towards three commercially independent business areas:

- The Network Owner of the passive network that provides the passive technology: e.g. empty conduits, fibre optics or copper wires, passive distributors.
- The Network Operator that provides the active technology, operates the network, and conveys the services to the end customer.
- The Services Provider who supplies and markets the services: telephony, Internet, TV, other added value services.

In real world conditions network owner and network operator partner with one another. However there will be many Service Providers that can offer their product portfolio in parallel via the same network access to the end consumer.

Dividing the business model horizontally allows other service providers to give their end-customers access to their portfolio. This extends the options open to end-customers. Competition emerges between the service providers and the new network access becomes more attractive to end customers. To the open-access network operator this means that, in comparison to the classical vertical business model, network utilization is increased significantly and financing is therefore easier and safeguarded.

In the future it is also conceivable that a company could adopt several roles on the open access market. Therefore, in open access business relationships it is important that no discrimination is made as regards access between each of the business areas, or in another words no preferential treatment is accorded.

The following figure shows the OAN model.

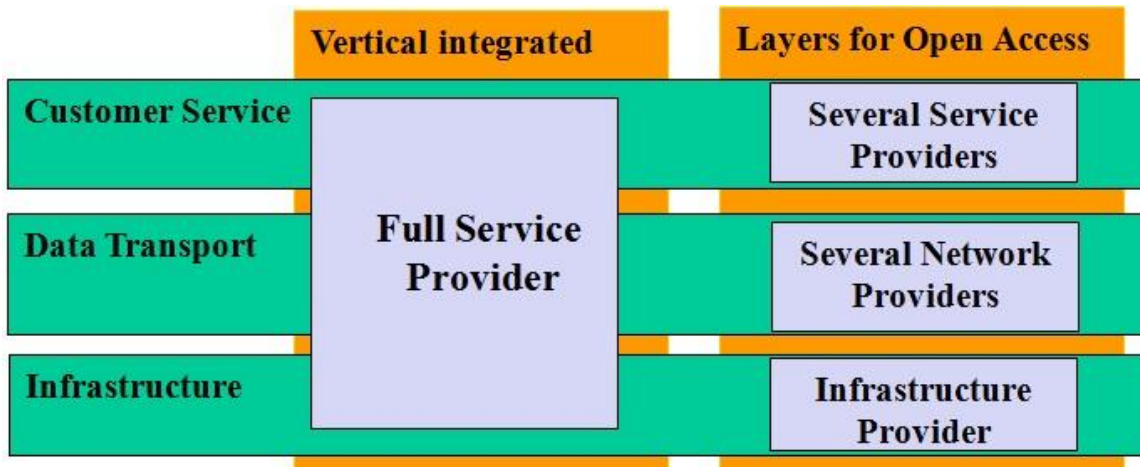


Figure 7: Open Access Network (OAN) relationship model

As shown in the following typical OAN topology, all RSPs can provision services to end users through the wholesale service over the OAN. The ARN provides different service channels for different RSPs, and the RSPs can select L2 or L3 devices for service access. The end user can

use only one physical port to flexibly choose RSPs according to service tariff and experience, and need not concern about the actual network connection.

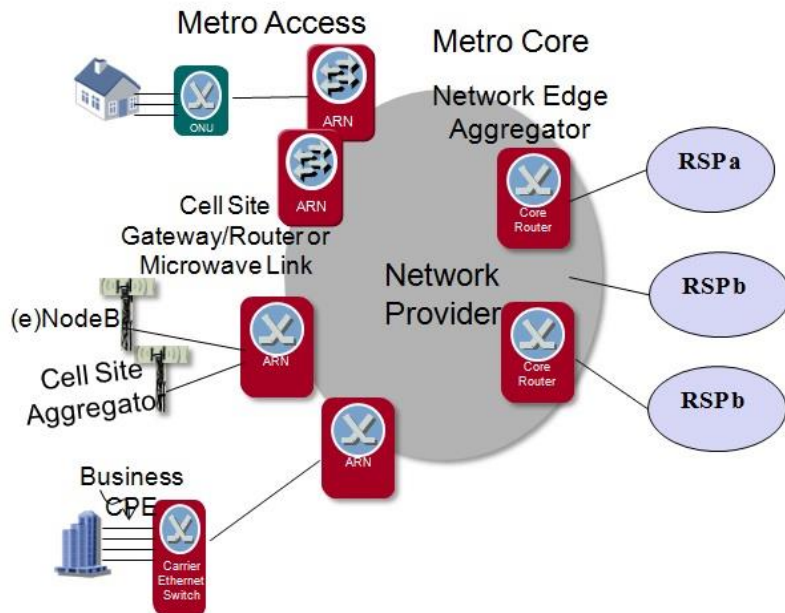


Figure 8: Typical OAN topology featuring ARN functional nodes.

Joint usage does of course place special demands on the systems in the access area that did not exist before the introduction of open access. Therefore, the above-mentioned specifications for network interconnection also entail new functionalities for the devices to be used in the access network.

For example, these are just some of the demands:

Layer 2 functionalities:

- Transmission of Tunnel Tag: Double-tagged VLAN services, MAC in MAC, MPLS TAG
- Using the entire VLAD address area
- Parallel operation of n:1 and 1:1 services

QoS service functionalities:

- Establishing service classes for voice, data and TV services
- Mapping of provider-specific service classes used

Traffic engineering functionalities:

- Bandwidth restriction of data streams upstream and downstream
- Broadband management for service classes – particularly for IPTV services
- Colour marking in combination with QoS classes to prevent blocking

Enhanced safety requirements:

- Separating the data between subscribers (basic demand)
- Additional separation of the data between providers

Enhanced multicast capabilities:

- Support of several multicast bodies by different providers
- Superior demands on the number of multicast streams possible
- Parallel operation of unicast and multicast
- Traffic engineering of multicast groups

These high demands require the enablement of long-term smooth operation in the open access environment. Thus, the ARN needs to provide several functionalities and features to support this operation model. The requirements of the ARN to achieve Open Access are mainly related to:

- Traffic isolation
- End-to-end customer management and segmentation
- Bandwidth and QoS

SODELES provides different interconnection services, which can be divided into optical-dedicated and electrical-bitstream transport. Each of them has a set of specifications that affect the requirements for an Open Access operation.

2.2.1 Optical transport

A dedicated wavelength service on SODELES has a low impact on the ARN as it acts as an optical filter to route the wavelength to the final customer. Ultimately, in a WDM-PON configuration, the ARN does not even receive the optical signal as it is routed through the previous AWG (see Figure 9).

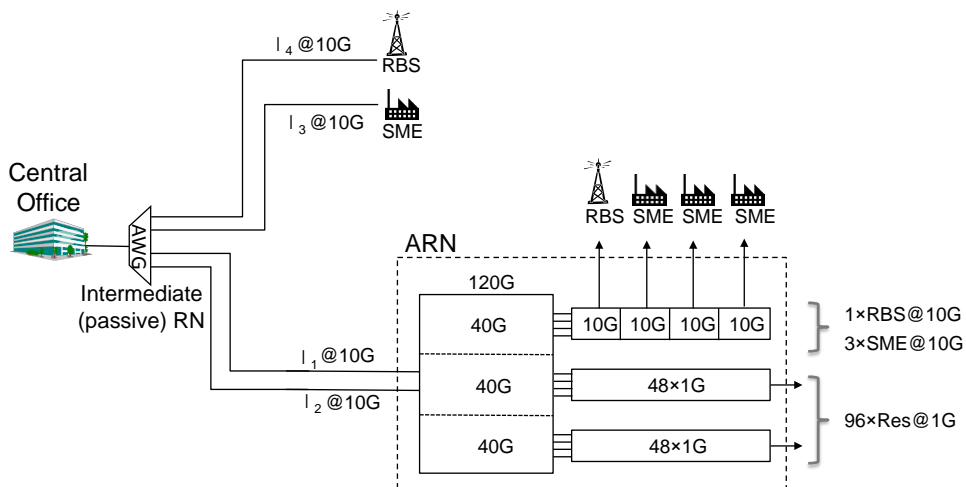


Figure 9: Dedicated wavelength service (ARN by-pass)

Additionally, a dedicated wavelength already provides inherently open access compatibility, as each wavelength is treated as an exclusive end-to-end service, so the pool of wavelengths can be assigned to different providers without any special requirement. However, a recommendation would be to assign a set of continuous wavelength to each provider (super channel) in order to manage the infrastructure more efficiently and also, have optical bands for dedicated wavelength services and others for bitstream transport.

Another consideration regarding the optical layer is the channel allocation and the number of wavelengths that can be injected in a single optical fibre. At present, 100-GHz and 50-GHz channel spacing is commercially available. Spacing of 12.5GHz and 25GHz are also under study. However, such narrow optical bandwidth plans limit the electrical bandwidth within the optical channel and in any case, the number of wavelengths is limited by the total power that can be injected in the fibre without generating non-linearities. Therefore, as SODALES follows a low-cost approach, 100-GHz channel spacing (allowing 40 wavelengths in the C-band) and 50-GHz channel spacing (allowing 80 wavelengths in the C-band) will be the preferred choices to be used in the optical transport layer.

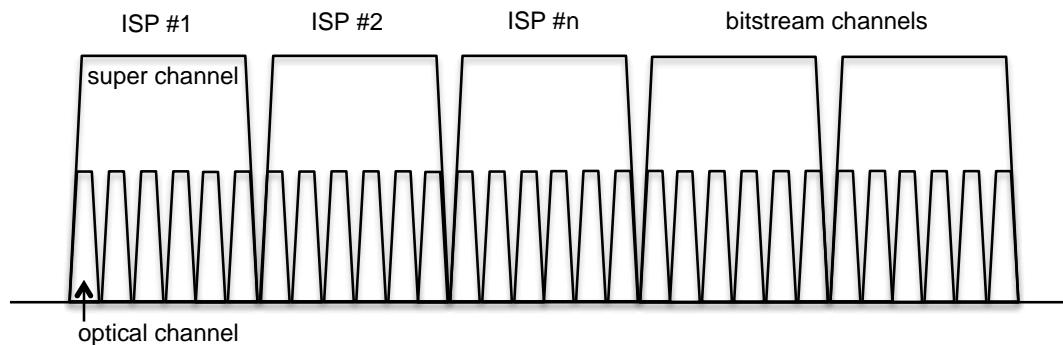


Figure 10: Wavelength segmentation

2.2.2 Electrical-bitstream transport

For electrical-bitstream transport, the ARN is a key device, which needs to support Open Access functionalities. The ARN connects residential users, businesses and RBS to the network and each of them may belong to different ISPs. Therefore, customer identification, segmentation and QoS are key within SODALES. As SODALES implements statistical multiplexing features at the ARN, also, non-discriminatory policies need to be defined to guarantee fair access to the upstream channels.

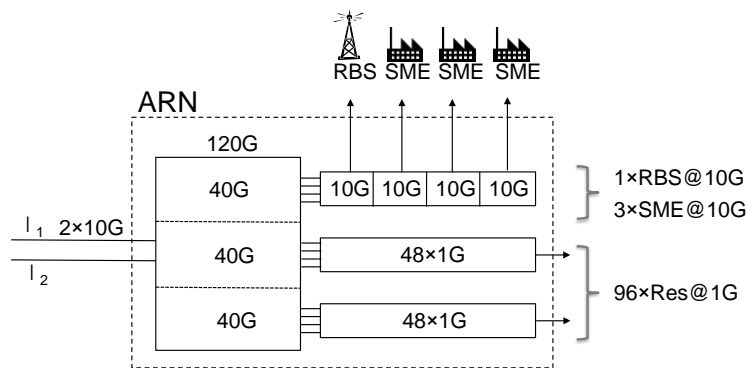


Figure 11: ARN interconnections

The SODALES architecture needs to support the required functionalities to offer Open Access features, which are:

- Scheduling hierarchies: port, service provides (logical port), user, priority
- E-Line
- E-LAN
- E-Tree
- APS

Together, these will provide the required traffic isolation, end-to-end customer management and Quality of Service. The service provider and the end-user coordinate between them the required service in terms of standardized service types and service attributes. These Carrier Ethernet service types are fundamental to the Carrier Ethernet service model and are defined in MEF 6.1.

2.2.2.1 E-Line

An E-Line is a point-to-point Ethernet service that connects 2 UNIs. Those 2 UNIs can communicate only with each other.

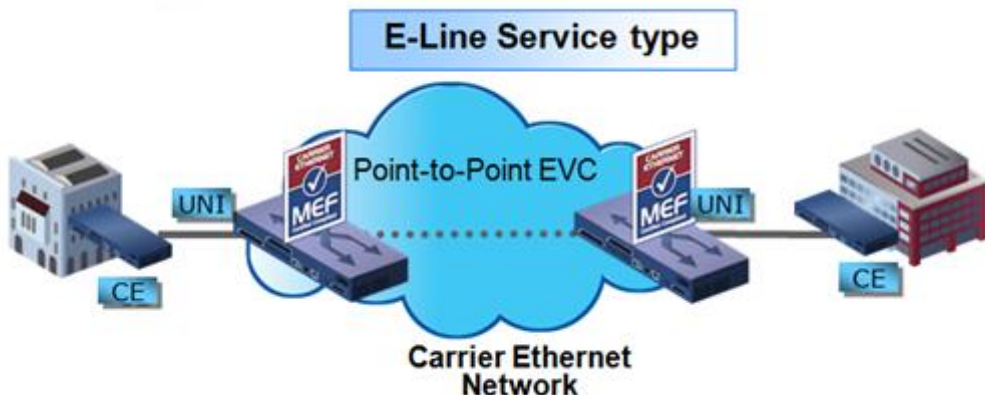


Figure 12: E-Line service type: point-to-point

E-Lines are used to create:

- Ethernet Private Lines
- Ethernet Virtual Private Lines
- Ethernet Internet access

For example, it can be used to replace TDM private lines. E-Line is the most popular Ethernet service type due to its simplicity.

2.2.2.2 E-LAN

An E-LAN is a multipoint-to-multipoint service that connects a number of UNIs (2 or more) providing full mesh connectivity for those sites. Each UNI can communicate with any other UNI that is connected to that Ethernet service.

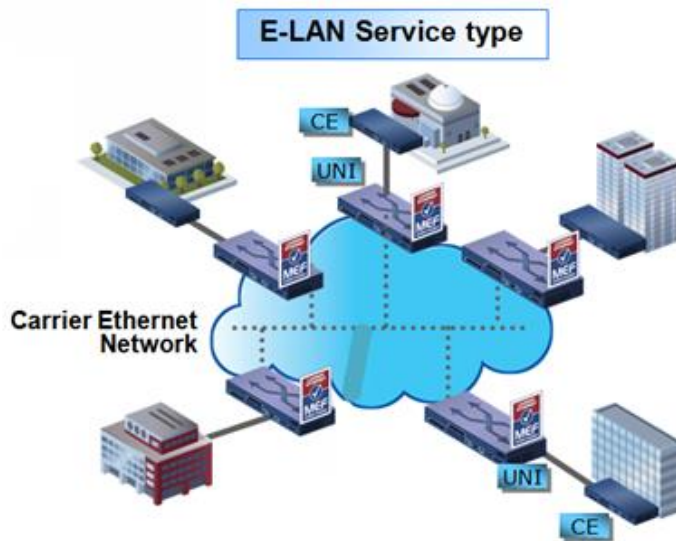


Figure 13: E-LAN service type: multipoint-to-multipoint

E-LANs are used to create:

- Multipoint L2 VPNs
- Transparent LAN services
- Layer 2 VPNs (L2VPN)
- Foundation for IPTV and Multicast networks

2.2.2.3 E-Tree

An E-Tree is a rooted multipoint service that connects a number of UNIs providing sites with hub and spoke multipoint connectivity. Each UNI is designated as either 'root' or 'leaf'. A root UNI can communicate with any leaf UNI, while a leaf UNI can communicate only with a root UNI.

E-Trees provide the separation between UNIs required to deliver a single service instance in which different customers (each having a leaf UNI) connect to an ISP which has one or more root UNIs. Having more than one root UNI is useful for load sharing and resiliency schemes.

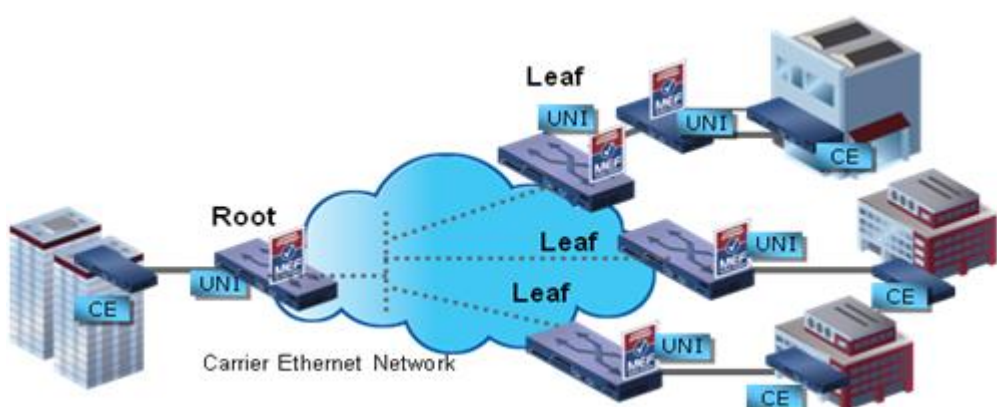


Figure 14: E-Tree with hub-and-spoke multipoint connectivity

E-Trees are used to create:

- Multicast delivery services
- Internet access
- Mobile backhaul services
- Telemetry services

Difference between E-LAN and E-Tree

E-LAN services are appropriate when all UNIs can generate traffic towards any other UNI and all UNIs belong to the same administrative domain - in other words when traffic separation between different organizations sharing the service is not required.

E-Tree services are appropriate when the service source is located at just one UNI, or a small number of UNIs, each of which is designated a root UNI. The end-users of the service are typically client organizations that require that their respective traffic will not be visible to other clients of the service.

Root vs. Leaf

In E-Lines and E-LANs, all UNIs are designated as a root UNI.

In E-Tree, UNIs are designated either as root UNIs or as leaf UNIs. Root UNIs are used to source traffic that can be directed to any other UNI in the E-Tree. Those UNIs should be only able to see traffic that originates in one of the root UNIs in the E-Tree are designated as leaf UNIs.

For example in an E-Tree used to provide access to multiple organizations to a single ISP, the ISP POP will sit at the root UNI, whereas each organization accessing the ISP sits at a leaf UNI so that it is unable to see traffic to and from other ISP clients.

Multiple root UNIs are permitted in E-Trees in order to support mirror sites (resiliency) and load sharing configurations.

2.2.2.4 Traffic isolation

In an Open Access Network, it is mandatory to correctly isolate users, especially those from different service providers. At present, there are several technologies to perform this, which, at the same time, offer scalability and bandwidth management.

The ARN needs to provide this, by supporting the technologies that can handle traffic from/to different sources totally isolated.

2.2.2.5 End-to-End customer management

Another of the SODALES key features is to allow ISPs to efficiently manage their customers. One of the weak points of Open Access networks is the lack of control of the customers by the ISPs, as the bitstream provider is the one that manages the connectivity between the customer premises and the Point of Presence (PoP).

The ARN need to allow ISPs to manage their customers and provide access to OAM for their customer traffic. Both, Carrier Ethernet and MPLS-TP provide functionalities to manage services

in the access segment. Carrier Ethernet offers two possible implementations, which are Y-1731/CFM and Ethernet First Mile, being the first more complete and also offering performance monitoring features. MPLS-TP offers now more limited fault management, which consists on basic heartbeats (BFD) and diagnostics (LSP-ping). RFCs 6374 and 6375 define a set of performance monitoring functions to be implemented over MPLS-TP.

2.2.2.6 Quality of Service

The ability to manage Quality of Service is also mandatory in Open Access networks (and in general, in Carrier networks) and therefore, the ARN need to support this feature. Also, control over the QoS needs to be transferred to the ISP so they can control the Quality of their flows (without interfering with the QoS of the other ISPs).

2.3 Traffic Management Technologies

Since SODALES is designed to have OAN capability, when considering the traffic management aspects, we need to take into account that it is an open architecture with a core concern for how to build a platform in which residential users can be equally and freely connected to multiple Service Providers. In this case, leasing L2 connection and bandwidth through the OAN is a basic feature of the OAN. To support L2 connection and bandwidth leasing, the active ARN must provide multiple and flexible upstream ports, multi-layer VLAN forwarding and transforming, and hierarchical QoS (HQoS) support. OANs of certain carriers manage only the network from the ARN to the ONT (including the ODN), and the upper layer devices of the ARN and lower-layer devices of the ONT (such as the home network devices) are all provided by the RSPs. Generally, different RSPs use different upstream ports, but one RSP can use multiple upstream ports. Different RSPs use different ports; therefore the RSPs can have the entire VLAN address space, and VLAN addresses of different RSPs may overlap.

In this project we are studying the use of a hierarchical QoS engine to solve these problems by supporting multiple levels of scheduling. The first level scheduler feeds traffic to the next level and that feed to the third level. With each of these schedulers, a separate classification and scheduling algorithm can be applied at each level. The first level scheduler can classify traffic into flows (e.g. coming from a specific host or a group of hosts). The second level can classify them based on services (e.g. whether it's VoIP traffic or normal Internet traffic), and third level scheduler can classify it based on Trunks associate to Regional Service Provider (i.e. a trunk going from location A to B and another going from A to C but sharing the same Egress port).

Hierarchical control is performed for services, users, and RSPs. As such, HQoS ensures bandwidth of all users and bandwidth of different services of each user through the hierarchical scheduling mechanism. The protocols and specific traffic management strategies and algorithms are discussed in greater detail in the parallel deliverable D1.3 "SODALES OAM and Control Plane Parameters for Open Access Networks" which accompanies this particular deliverable. In addition, the later deliverables (month 12) D3.2 "OAM Parameters Design for E2E Service Delivery" and D3.3 "Control and Management Plane Design" will also be offering much greater detail of the implementation strategy of the SODALES traffic management strategy, specifically where it relates to the design of the ARN. In section 5 of this deliverable, we also describe some initial simulation results of an efficient flow scheduling approach that can also be employed to enhance traffic management capability at the ARN, and shows promise for improving average throughput and reducing configuration delays.

2.4 Meshing & Resilience

Although access networks typically present a limited set of resilience features, SODELES can be implemented in resilient configurations to provide enhanced protection and higher availability. The ARN is a key component to provide this feature, as it is the active element that aggregates the traffic from the users and transmits it to the CO depending on different parameters. Mesh and resilient configurations can be implemented at the optical or electrical domain, but in both cases, the SODELES control and management plane will need to interact with the ARN so the flows are correctly transmitted.

2.4.1 Optical resiliency

The generic approach to offer optical resiliency is by implementing ROADM s at the ARN. Optical resiliency is the best future-proof alternative but requires extra power and the implementation cost of an optical mesh is high. As SODELES aims to be a cost effective approach for future access networks using low-energy subsystems, the ROADM path is not the preferred choice.

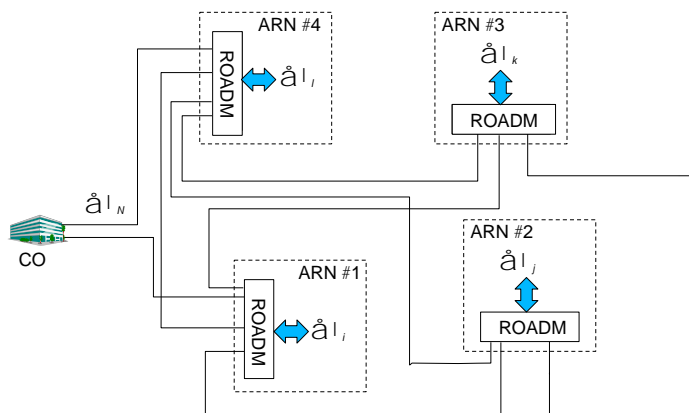


Figure 15: Optical mesh topology

Therefore, other configurations with L1 resiliency better fit within SODELES vision. A simplified way to offer resiliency is to use a fixed OADM approach. The principle is to deploy a SODELES ring and allocate two wavelengths to each ARN, each of which is transmitted from/to one direction of the ring.

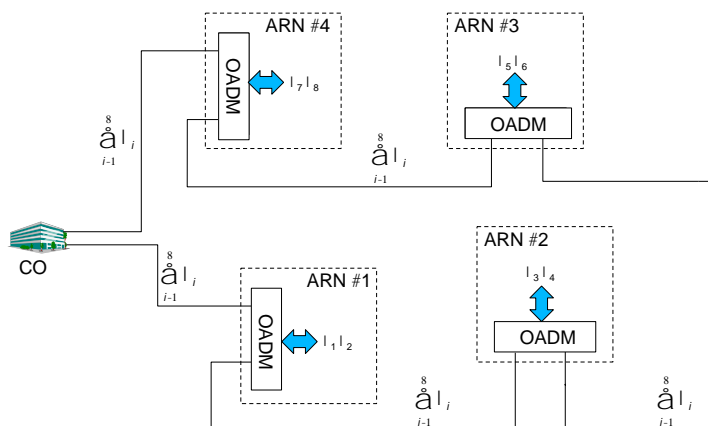


Figure 16: OADM resilient topology

This approach has zero impact in power consumption, as it just uses passive components and the impact on cost is low, as just a basic optical filtering layer is required.

In case of a fibre cut, the ARN reduces throughput in 50% but connectivity is guaranteed by the connection that remain between the ARN and CO.

Mesh configurations are also possible but the logical connection from the CO to the ARN will keep being a ring with two interfaces through two different physical paths.

2.4.2 Switching resiliency

Basic protection can also be implemented by daisy-chaining several ARNs one to each other.

This architecture provides a common interface to the CO, which means that the group of ARNs connected in the chain shares a bidirectional 10 Gb/s ring (20 Gb/s total capacity).

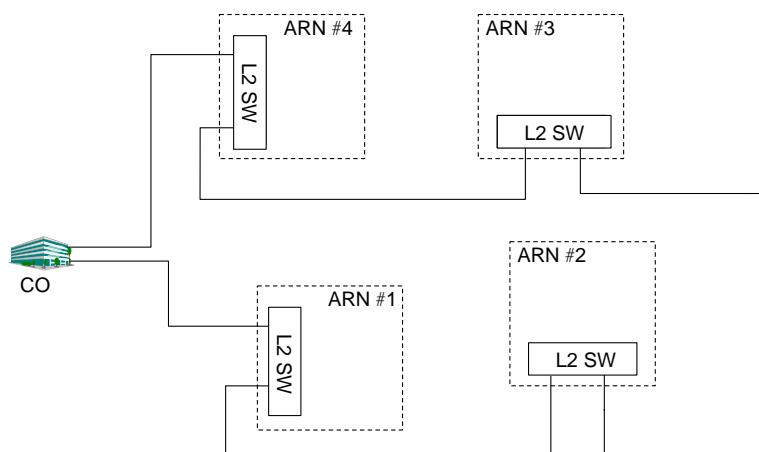


Figure 17: Electrical mesh topology

In order to efficiently switch traffic flows and avoid loops, L2 features, like Spanning Tree protocols need to be implemented.

However, this is not seen as a future-proofed approach and also limits the total capacity of the network. That said, an advantage of this approach is that it allows geographic bandwidth allocation to specific ARNs depending on the traffic needs.

3 Wireless Final-Drop Technologies

An important aspect about the wireless (RF and optical) final-drop technologies being developed in the SODALES project is that it additionally provides an enabling tool for next-generation heterogeneous wireless and mobile broadband systems, based on flexible spectrum usage, reduced EMF and interference. Figure 18 below shows how, in a more generic fashion, the wireless final-drop SODALES technology can contribute strongly to future heterogeneous architectures. In this particular (more forward-looking) context, it is anticipated that both cellular and WiFi standards will continue along the OFDM track for the physical layer, with enhancements to achieve higher speeds approaching 100–1 Gb/s for cellular mobile and nomadic use, respectively, and 1 Gb/s for WLAN in home and office environments. Proposed enhancements include the use of dynamic spectrum access (DSA) and non-contiguous OFDM to achieve wideband operation, increasing numbers of antennas or beams, network MIMO involving cooperative signal processing between base stations, and cooperative communication techniques in general. With modulation efficiency presently regarded as reaching its practical limits, an enabler for higher speed data will be the availability of wideband channels using advanced DSA and cognitive radio techniques. All of these features may be additionally exhibited in the final SODALES final-drop design.

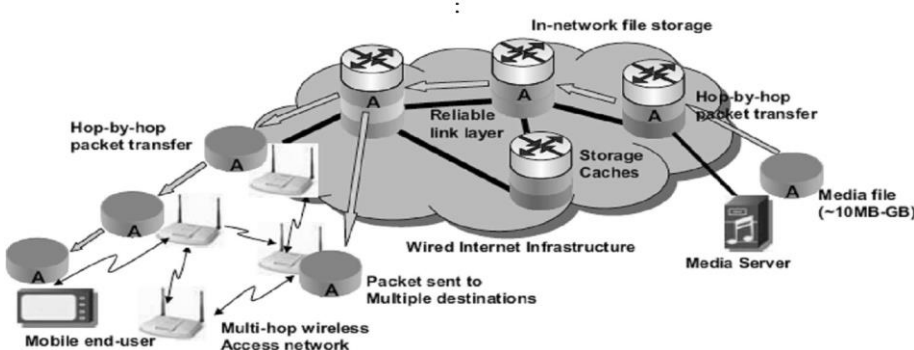


Figure 18: Cache-and-forward network architectures featuring high-capacity wireless networks [15]

There is also on-going effort to migrate indoor WLAN and WPAN networks towards less congested higher frequency unlicensed spectrum bands such as V-band and E-band. There are significant propagation-related differences between the V/E bands and the lower frequency unlicensed WiFi bands at 2.4 and 5.0 GHz. Several standardization bodies have been working on the V-band PHY and MAC protocols approaching 1-Gb/s service rate. These include the IEEE 802.11ad and Wireless Gigabit Alliance (WiGig) for WLAN, and IEEE 802.15.3c, and Wireless HD for short-range PANs. The IEEE 802.15.3c standard defines a central controlled network topology and TDMA-based MAC protocol for 60-GHz wireless PANs. The IEEE 802.11ad standard has introduced a new network architecture named Personal Basic Service without an access point, in which each station can serve the role of a central coordination point which supports a combination of random access CSMA access and scheduled TDMA access modes. There are still a number of open research issues related to 60-GHz networks such as MAC-layer support for beam switching, diversity techniques to overcome propagation impairments,

cooperative relaying. Overall, 60-GHz technology is expected to mature rapidly during the next three to five years and will provide an important option for high-speed connectivity associated with applications such as device docking, HD video and mobile caching, in addition to the ubiquitous connectivity as shown in Figure 18.

In terms of hardware technologies, wireless PHY and MAC technologies discussed in this section involve considerable signal processing complexity, generally requiring ASIC implementation in order to achieve the (theoretical) gigabit throughput associated with radio standards such as 802.11ad and 802.11ac at low cost. The high cost of chip development implies the need for mass-market standards with significant volume in order for a new product concept to be viable. This in turn results in relatively long product development cycles of seven to ten years in the wireless industry, as compared with three to five years in the computer industry, which relies on processors, memory, and other generic components that do not require completely new architectures for each generation. A suggested scenario is shown below in Figure 19 [15].

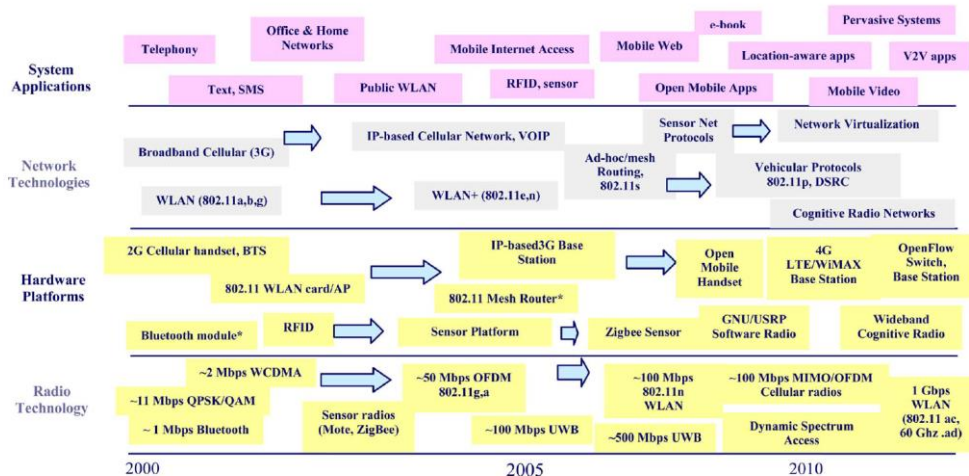


Figure 19: RF technology application scenarios into 2015 and beyond (adapted from [15]).

To achieve these ambitious end application scenarios, the following sections describe the present progress in connectivity between end-users (fixed and mobile), data caches and distribution hubs in the following key technology areas:

- High capacity wireless backhaul
- High spectral efficiency (SE)
- Low-cost components
- Real-time signal processing
- Reconfigurable radio systems (RRS)
- Line-of-Sight (LOS) optical

The driver behind these advances is the roadmap set by Ethernet wireless connectivity, whereby 100 Gb/s throughputs have recently been achieved with mm-wave photonic links, e.g. [22]. Set against this, pure radio-based throughputs featuring freely available, license-free/light-license

spectrum allocation (at 2.4, 5, 24, 60, 70 and 80 GHz) do not presently align well, even with the 10GbE copper twisted-pair base standard 802.3an-2006. It may also be noted that deployment of 10GbE in metro/access networks is rapidly displacing legacy SONET OC-48 and OC-192, as 10GbE enables service providers to quickly address the unpredictable and rapid growth in bandwidth; this is fuelled in part by increased bandwidth demand from mobile users. In a wider scenario, one can also include the convergence of high-speed Internet, digital home phones, and television services. These are creating additional bandwidth demands per household on a single access line surpassing 12 Mb/s. It is also important to note that emerging LTE mobile services have a minimum 100 Mb/s Ethernet requirement.

3.1 High-Capacity 60-GHz Wireless Links

For licence-free spectral usage, a wide-range of commercial back-haul links at 24 and 60 GHz are on offer, with transmission distances >20km possible. Under clear air conditions, atmospheric attenuation varies significantly with frequency, in addition to conventional free-space path loss [26]. At microwave frequencies up to 38 GHz, atmospheric attenuation is reasonably low at a few tenths of a dB/km. A large peak is seen at around 60 GHz of ~15 dB/km where absorption by oxygen molecules seriously limits radio transmission distances. After this peak, however, a large window opens up where attenuation drops back to 0.5 dB/km—not much worse than at lower mm-wave frequencies. Above 100 GHz, atmospheric attenuation generally worsens and there are numerous molecular effects (O_2 and H_2O absorption at higher frequencies).

Figure 20 shows a typical 60 GHz 1GbE full-duplex link [27]. A more recent addition is represented by an affordable commercial 24 GHz solution as shown in Figure 21 [28]. The 24 GHz band has few issues with atmospheric attenuation. However, the allocated bandwidth is just 200 MHz as this band was primarily intended for automotive radar [29]. The use of 2x2 multiple input/multiple-output (MIMO) together with hybrid frequency/time-division multiplexing is indicative of current advanced trends in mm-wave links. These include: multiple frequency bands, spatial MIMO, high-level QAM constellation ([28] uses 64QAM) and, for predominantly LOS deployments, polarization diversity. For mobile backhaul, 60 GHz has attractive features for short small-cell LOS backhaul links: It is unlicensed, offers wide bandwidths, and has high path attenuation due to the oxygen resonance peak. 60 GHz is useful for short hops and high frequency reuse. Recently e.g. NEC stated that the 60 GHz band was their main path for wireless small cell backhaul [30].



Figure 20: 60 GHz 1GbE backhaul link [27].



Figure 21: 24 GHz, 1GbE backhaul link [28].

Concerning licensed bands, microwave is the most common mobile backhaul technology nowadays, transporting more than 50% of the global mobile traffic. Most installed links use point-to-point LOS links between 6 and 42 GHz and bandwidths of 3.5, 7, 14, 28, 56, and 112 MHz. Wider channels are available at higher frequencies and by aggregating multiple bands. For example, the licensed 70/80 GHz band offers 250 MHz channels possible to aggregate. Using wide bandwidths and high spectral efficiency tens of Gb/s wireless throughputs are within reach. These bitrates were historically considered viable only by using optical technologies such as fibre. A 5-Gb/s microwave link was demonstrated by Ericsson at MWC in Barcelona 2011.

Although the SODEALES architecture is designed to exploit WDM-PON infrastructure for the upstream backhaul functionality, the high-bandwidth (1 GHz) capacity of a RF final-drop technology solution could also find application for backhaul capability, or for inter-ARN meshing functionalities, e.g. for network resilience and restoration.

3.1.1 Spectral Efficiency

The physical path design of the Ethernet twisted-pair copper media standard 10GBASE-T (802.3an) represents one of the most advanced constellations in common use at very high symbol rates. As shown below in Figure 22, each of the four channels uses an 800 Mbaud symbol rate with 3.125 bits per DSQ-128 dimension, giving 2.5 Gb/s/copper pair. This is derived using 16-PAM at 4 bit/dim, which is reduced to 3.125 bit/dim by 2-D alphabet partitioning and coding. The cable transmission matrix is highly cross-linked, suggesting that MIMO-OFDM could be used. However, latency issues make this a poor choice; a factor often overlooked in the use of OFDM signaling. The use of intrinsic echo and cross-talk cancellation offers a strong (and essential) advantage in signal-to-noise ratio (SNR). Overall a BER of 10^{-12} is achieved with a SNR of 23.32 dB. A low-density, parity check code (LDPC [2048,1723]) offers 8 dB coding gain.

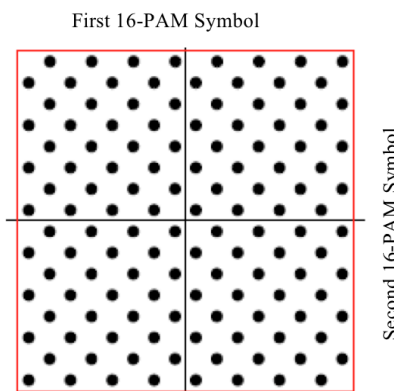


Figure 22: DSQ-128 Modulation.

For microwave mobile backhaul, over the last ten years, state of the art spectral efficiency has increased from a modest 1.2 b/s/Hz to a record value of 35 b/s/Hz demonstrated by Ericsson at the Mobile World Congress 2011 in Barcelona. Enabling technologies for such an increase in spectral efficiency are MIMO technologies such as polarization multiplexing and spatial multiplexing, and high order modulation where 512QAM is commercially available and 1024QAM and higher are to be introduced to the market [31]. Recent records in spectral efficiencies achieved in optical communications e.g. over multi-mode fibres, rely all on off-line processing after sampling the signals in a high-speed oscilloscope.

3.1.2 MIMO at mm-wave frequencies

The idea of using multiple antenna techniques also denoted as multiple-input multiple-output (MIMO) for increasing the data rates powered more than a decade of research and innovation in mobile communications. MIMO is introduced into the wireless local area networks (LANs) standard 802.11n. Integration of MIMO into the cellular world, namely the 3G High-Speed Downlink Packet Access (HSDPA) was tried early. But realizing the gains turned out to non-trivial due to the fundamental interference limitations. For improving the performance, efficient solutions going beyond these limitations are needed. Modern solutions are based on orthogonal frequency division multiple access (OFDMA) and single-carrier frequency-division multiple access (SC-FDMA). These waveforms have been incorporated into the new 4G LTE standard for down-link and up-link, respectively, since they reduce complexity at the receiver side dramatically.

At mm-wave frequencies, however, MIMO has played no role so far. One reason is that most links are based on line-of-sight (LOS), where polarization multiplexing is an efficient way to double the channel rank using the same antenna configuration. At microwave frequencies, however, it is difficult to gain more degrees of freedom using LOS over large distances since antenna elements cannot be spaced close enough for creating a rank-deficient MIMO channel.

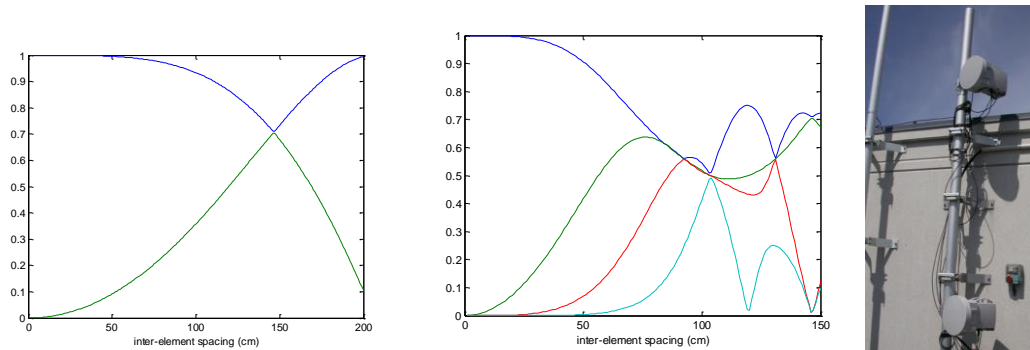


Figure 23: Singular values of MIMO modes versus the inter-element spacing in 70 GHz mm-wave link after 1 km distance. Left: 2x2 MIMO with linear arrays at both sides. Centre: 4x4 MIMO with linear arrays. Right: 2x2 LOS-MIMO from [40].

However, researchers have demonstrated theoretically [32] and practically [33][34][35][36][37][38][39], that smart antenna configurations imply that the mm-wave MIMO channel can have full rank. In Figure 23, singular values characterizing the relative strength of the parallel MIMO streams for 2x2 and 4x4 antenna configurations are plotted at 70 GHz versus the inter-element separation after 1 km link distance. Obviously, already with distances in the order of one metre, we can multiplex four data streams spatially over the LOS channel. The number of streams is doubled by using polarization multiplexing. In practice, multiple dish antennas can be placed vertically on top of each other at an antenna mast.

The authors in [37] used an analogue combining circuit at IF frequencies to separate spatially multiplexed data streams at 60 GHz. However, bandwidth was noticeably limited. The authors in [33] already used single-carrier real-time signal processing and achieved 700 Mb/s with 4 elements in an indoor environment at 5.2 GHz. Note that parallel streams are degenerate only at a given frequency and at a specific inter-element spacing. For realizing a high-bandwidth mm-wave MIMO link, frequency-selective MIMO processing will be needed. The authors in [39] recently implemented a 1 Gb/s MIMO-OFDM microwave link at 15 GHz. However, bandwidth was limited by signal processing of the standard PC platform and by interfaces used.

3.1.3 Low-cost Components

The market for mm-wave components such as amplifiers, phase-locked loops and mixers has been steadily growing with the advent of 1 GbE links such as those in §3.1 above. As shown in Figure 24, highly integrated transmitter and receiver MMICs have been designed in a commercial 65nm 183-GHz GaAs pHEMT MMIC process and characterized on both chip and system level. These chips show a high level of integration in the 60-90 GHz bands and offer useful multipurpose front-end designs.

The chips operate with a LO signal in the range 10-20 GHz which can be up-converted in an integrated multiply-by-four/eight chain, whilst offering IF centre frequencies up to 8 GHz. Although the chips are inherently multipurpose designs, they are especially suitable for high-speed wireless data transmission due to their very broadband IF characteristics. A single chip transmitter MMIC might consist of a balanced resistive mixer with an integrated ultra-wideband, IF balun, a three-stage power amplifier, and the X4/8 LO chain.

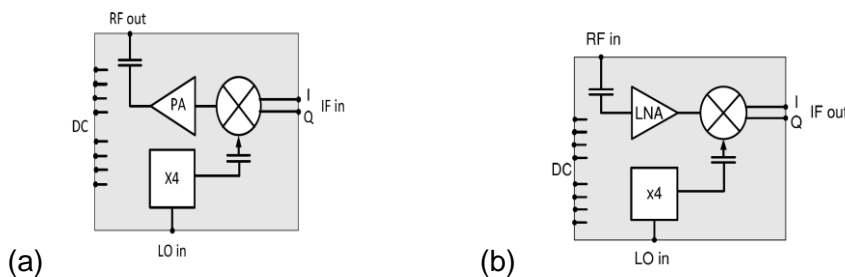


Figure 24 (a) & (b): Examples of 60-90 Hz mixer chips [40].

3.1.4 Real-Time Signal Processing

There have been a number of real-time processing GbE wireless systems published. As an example, Figure 25 shows an untested design concept of a complete wireless system for 60 GHz [41]. This proposed two-chip solution follows broadly conventional functionality, so just the main features are summarized. Following the 1GbE PHY input, the signal is LDPC encoded (as in 10GBASE-T above). This is then split into I and Q symbol streams and up-converted on 5.1 GHz sub-carrier and then re-modulated onto a 54.7 or 57.1 GHz carrier as shown.

This produces a frequency division-duplex (FDD) signal at either 59.8 or 62.2 GHz; this helpfully allowing diplexer rather than circulator-based Tx/Rx signal separation at the final antenna output. At the receive side, the reverse process happens. Not shown is the necessary synthesizer lock on the 1st and 2nd down-conversion PLLs. Additionally, I and Q signal phase rotation has to be removed by the base-band receiver, in addition to synchronization of the LDPC codec frames. Much of this effort can be migrated to standard 10GBASE-T and forthcoming 40GBASE-T network interface cards.

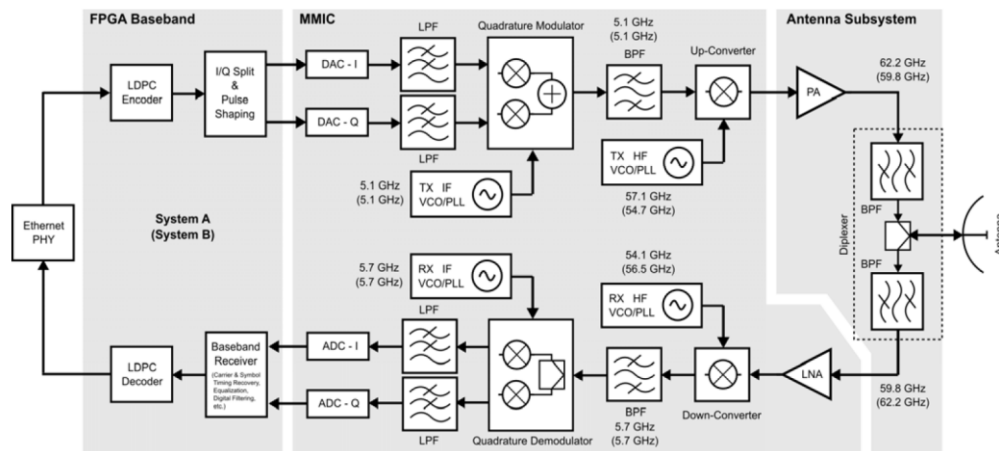


Figure 25: Schematic 60 GHz GbE real-time wireless system [41].

3.1.5 Reconfigurable Radio System (RRS)

Reconfigurable radio is a state-of-the-art requirement for wireless links in general. In case of microwave, propagation conditions change, due to the weather. Moreover, radio links are supposed to create little interference and be energy-efficient. If the traffic is temporarily low, we can adapt power consumption and throughput, accordingly. Such adaptation may include the use of less complex modulation formats, waveforms better adapted to lower spectrum efficiency and adaptation of the spectrum utilization.

Figure 26 shows the various elements of a RRS, which perform its reconfiguration management operations. The joint radio resource management element is responsible for coordinating the negotiations between reconfigurable network elements, and for ensuring that the optimal utilisation of radio resources by all network elements is achieved.

The radio access technologies (RATs) in each network element possess their own individual resource management, mobility management, and other link control mechanisms, which are in turn defined within their RAT standards. The RRS's reconfiguration management system interfaces with these mechanisms, thereby enabling it to adjust the radio resource utilisation of each network element. A network operator is able to exercise control over reconfiguration operations through the use of policies, which provide network elements with a set of predefined reconfiguration objectives and restrictions. Policy-based management is also beneficial, as it enables the autonomous reconfiguration of network elements without requesting/obtaining permission from the network operator in the core network.

Dynamic spectrum access/allocation (DSA) enables the dynamic allocation of spectrum to accommodate each reconfigurable network element, and in so doing ensures both efficient use of the available spectrum, adherence to national spectrum licensing regulations and best energy efficiency. DSA elements in separate RRSs can also conduct negotiations, thereby enabling spectrum leasing and sharing.

The main challenge in this context is three-fold. We need a reconfigurable user plane, i.e. a functional pipeline doing all the signal processing from data bits to waveforms at high signal processing speed. To our knowledge, the highest symbol rate ever handled within an adaptive user plane is in the research prior to LTE, where 100 MSymbols/s processing was used to achieve 1 Gb/s [43]. This research direction was halted since the maximum symbol rate for LTE

is 30.72 MS/s. More recent work on NLOS 60 GHz using MIMO demonstrates that it is in fact scalable to much higher speeds [44].

The second challenge is an intelligent control plane. It can be split into two parts. First, we need a digital signal processor operating an intelligent algorithm. The control plane algorithm supervises the pipeline realizing the user plane. Second, we need reliable feedback and control channels. They are operated between the supervising processor elements at each radio frontend over the air in parallel to the user plane data. They enable the information exchange required to optimize the transmission with respect to channel conditions in radio link and traffic conditions in the network.

The interaction between user and control plane in an adaptive MAC processor is readily implementable in real-time on a reconfigurable signal processing platform e.g. for LTE, see [45]. MIMO-OFDM has inherently high potential for parallel and pipelined signal processing.

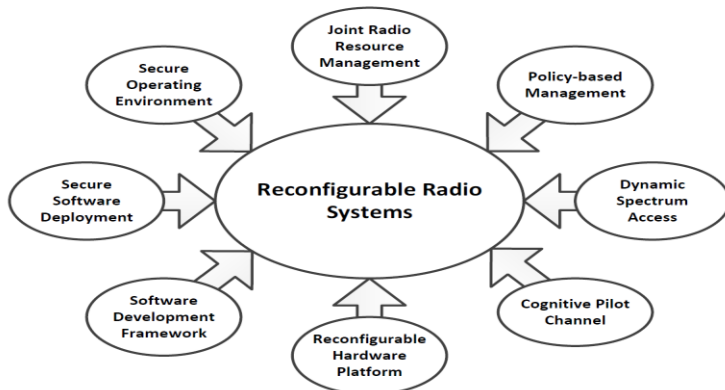


Figure 26: Key functional elements associated with reconfigurable radio systems [42].

Due to the reconfigurable nature of mobile devices (RMDs) and reconfigurable base stations (RBSs), establishing communications between these network elements is impossible if the RMD is unaware of the RAT currently implemented by the RBS [42]. This problem is resolved by the concept known as a cognitive pilot channel (CPC). A CPC is a universal predefined logical communications channel, which enables a RMD to contact a RBS and determine which RATs may be implemented by the RMD in order to establish communications with the RBS [46].

Apart from facilitating initial communications between RMDs and RBSs, the CPC can also be used to convey all reconfiguration management messages within an RRS, or support negotiations for spectrum sharing from secondary users of licensed radio spectrum. The CPC can be established as a logical channel over an existing RAT (in-band), or via a new RAT dedicated to performing this function (out-of band) [47].

To ensure interoperability between network elements and portability of software, an RRS must define a standardised interface that connects the reconfigurable hardware platform to the operating system and radio applications within each network element. This principle extends to the requirement for a standardised software development framework for radio applications. Such a framework enables radio application developers to create RAT software, which can be deployed on any network element provided that such elements contain hardware capable of meeting the software's performance requirements.

3.1.6 Line-of-Sight (LoS) Optical Solutions

3.1.6.1 State of the Art

The line-of-sight (LoS) approach, an example of which is shown in Figure 27 (left) was originally developed for military and space applications. In essence, an infrared laser (typically 1300-1550 nm to match atmospheric transparency) is directly modulated by the data signal; the output is collimated to achieve low-divergence and then collected by a large aperture lens [23]. The low-intensity received optical signal is then focused onto a high-speed, low noise photodiode and converted back to an electrical analogue for further processing. Error correction is usually applied to the regenerated digital signal such that a low-packet loss, full-duplex link (assuming an identical return path) is possible. In a terrestrial environment, the links work well and can provide in excess of 1GbE throughput over km distances.

The chief impairments (apart from simple obstruction) are due to Mie scattering from fog (which can be \sim dB/m) as well as from snowflakes and hydrometeors. The availability of LOS optical solutions is therefore not comparable to micro- and millimetre-wave solutions. Long-term measurements over 500 m distance using a commercial LOS optical link from CBL GmbH in the LTE-Advanced Testbed in Berlin illustrated outage events in the morning fog and during the typical November weather in Germany, when clouds hang deep and the 85 m high building at the Ernst Reuter Platz was covered, i.e. visibility approached zero.

In other weather conditions, the experience with LOS optical links is excellent, provided that beam alignment is optimal and the transceivers are mounted stable, e.g. at the bottom of a radio mast. Although omni-directional links and non-LOS (NLOS) applications have been reported, e.g. [25], they are limited to very short ranges simply because of the power budget.

From a network operator perspective, LOS optical links have insufficient availability for achieving macro-cell coverage due to atmospheric humidity. In order to improve availability, they are often combined with radio links serving as a back-up solution. LOS optics is currently considered as a temporal but not a sustainable solution for telecommunication networks where 99.99% availability is required. However, in the case where other solutions are not available, optical wireless is an alternative.



Figure 27: Left: A commercial line-of-sight link [24]. Right: Bidirectional optical wireless links based on LEDs, originally developed for indoor applications. For further information, see www.hhi.de

3.1.6.2 Small Cell Needs

Small cells are going to be massively introduced into the cellular network and will be embedded at locations where macro-cell coverage is available but capacity is insufficient because of high user density. Of relevance to the SODALES project is the fact that these small cells will also require an economic backhaul technical solution.

Since macro-cell coverage is always available, limited availability of perhaps 99% may be considered acceptable by network operators, provided that costs can be significantly reduced. Moreover, distances between macro- and small cells are shorter than between the macro-cells.

It is often said that 50% of the small-cell backhaul links have no free LOS. Obviously, there is a significant market for LOS solutions and the potential of optical wireless to compete with microwave in this market is better as compared to the macro-cell backhaul case because:

- the optical spectrum is free
- distances are shorter (few 100 metres) yielding higher weather margins
- limited availability may be acceptable if costs can be reduced
- availability may be increased by using adaptive modulation and coding

3.1.6.3 From visible light communications to low-cost wireless backhaul

Low-cost backhauling may become feasible with LED-based optical wireless links that have recently been mainly developed for indoor wireless access applications. In this case, the concept is based on the use of novel LED-based indoor lighting as a medium for communications. This idea has inspired researchers around world wide to reconsider optical wireless communications, since there is a potential for a mass market as LED lighting is becoming evermore widespread..

Improvements in transmission power, receiver sensitivity and energy efficiency have been reached recently in optical wireless communications, with LEDs nowadays providing output powers of several watts. There is progress in advanced impedance matching at the LED driver and at the photodiode yielding a better energy efficiency and high throughput at lower light levels. ASIC implementation of the baseband processing, instead of using FPGAs, further reduces power consumption. For indoor access applications, a few watts of optical power are needed to operate the link over a distance of several metres in a spot size covering a few metres. Two-thirds of the energy is needed for the LED bias current, while 1/3 is for the rest of the electronics.

For outdoor applications, we can use collimating optics, to yield the same spot size after several 100's of metres, as is typical for FSO links, and also using infrared LEDs instead of visible light. This will allow readily available VLC links to be converted into low-cost backhaul links by using essentially the same hardware, suitable for deployment in the SODALES architecture.

Compact prototypes are already available based on commercially available components. Currently, they feature data rates up to 500 Mb/s, with the clear potential of reaching several Gb/s, using an ASIC for baseband processing based on OFDM, as well as reliable feedback and control loops over the air enabling closed-loop rate adaptation according to the instantaneous channel conditions.

In wireless backhauling applications, such rate adaptation increases the availability, i.e. the link can still be operated under bad weather conditions and only the data rate is reduced, accordingly. This feature might qualify these links further for low-cost small-cell backhaul applications, provided that the LOS is free.

Low-cost LED-based optical wireless for backhaul applications is a new concept that needs to be proved in practice yet. However, there is no obvious reason why it should be infeasible. LED-based optical wireless promises an economic, energy-efficient, high-speed mobile backhaul solution covering a significant fraction of the existing small-cell scenarios, where a free LOS to an adjacent macro-cell is available.

Small-cell backhauling as well as wireless final drops are important applications covered by the SODEALES architecture. The use of optical wireless may have disruptive effects on the deployment costs, and turn into a serious business case if accepted by network operators. For this reason, it is a short-term research goal to modify LED-based LOS technology and to test it in real mobile network scenarios. In the following, we review recent VLC developments with a focus on high-speed data transmission and describe a recent hardware prototype [48].

3.1.6.4 High-Speed VLC Links

During the past few years, growing insights were gained into the efficient implementation of VLC data transmission using LEDs initially developed for illumination purposes. In general, there are two main types of white LEDs commonly used for lighting: the phosphorescent type consisting of a blue LED chip plus a yellow phosphor layer, and the multi-color type consisting of three (in some cases four) individual chips, mostly red, green and blue (hence: RGB). While the phosphorescent type allows for cost-efficient installations mainly due to its simple driver design, it provides only a few MHz modulation bandwidth caused by the slow response time of the phosphorescent material. However, we were able to demonstrate that the bandwidth can be enhanced by an order of magnitude up to 20 MHz by suppressing the phosphorescent portion of the optical spectrum with the aid of a “blue filter” at the receiver [5]. In contrast, the white-light RGB-type LEDs enable three individual color channels each providing approximately 15 MHz bandwidth. By using three drivers in parallel, wavelength division multiplexing (WDM) can be realized. However, the advantage of an increased aggregate data rate is achieved at the expense of higher costs.

We demonstrated that, although illumination LEDs are not developed for data transmission, they offer significant potential for high-speed communications. Starting with phosphorescent LEDs and simple On-Off Keying (OOK) modulation, which allowed 100-200 Mb/s data rates, the transmission speeds were increased continuously by applying more spectrally efficient modulation formats such as adaptive Orthogonal Frequency Division Multiplexing (OFDM) alias Discrete Multitone Transmission (DMT¹), an idea originally proposed in [49]. We continued working on sophisticated design and transmission improvements enabling up to 800 Mb/s using a standard high-brightness RGB-LED combined with a commercial Si-PIN-photodiode in a single-color transmission mode [50]. These results confirmed that ordinary RGB-LEDs designed for illumination can deliver data rates up to the Gb/s range based on DMT modulation with bit and power loading for throughput maximization beyond conventional 3-dB-bandwidth limitations.

A real boost of the throughput can be achieved with RGB-LEDs using WDM. The principle is shown in Figure 28. WDM for VLC was studied in detail in [49] using a commercially available high-brightness white-light RGB-LED as optical source and WDM pass-band filters combined with an APD as receiver element. The aggregate data rate was extended to 1.25 Gb/s at an illuminance level of 1000 lx at the receiver, a value within the range recommended by the European lighting standard (EN 12464-1 from 2003) for working environments. Based on a

¹ The DMT technique is known from DSL; whereas in radio systems it is known as OFDM. DMT can be realized using OFDM where a real-valued waveform is obtained using a so-called mirror function, see [7].

similar offline-processed WDM-VLC setup and a low-power RGB-LED, authors in [9] reported an aggregate data rate of 3.4 Gb/s. More recently, 3.22 Gb/s have been demonstrated using WDM-VLC with carrier-less amplitude and phase (CAP) modulation [10].

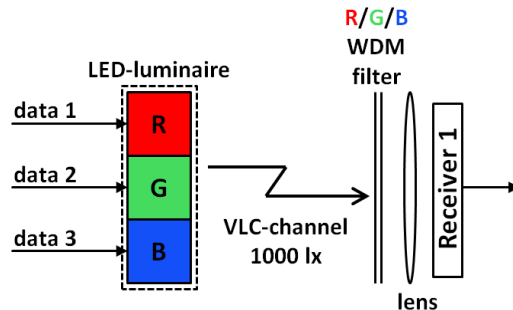


Figure 28: WDM principle for VLC showing in-parallel transmission of three (RGB) channels and reception of one channel via color filtering.

3.1.6.5 Real-Time 500 Mbit/s Bidirectional VLC Prototype

Besides the high-speed, off-line processed laboratory achievements, the maturity of VLC technology for all the potential applications has to be proven with real-time systems, an effort onto which we focused recently. The very first fully-fledged VLC real-time demonstration was presented in February 2011 at ORANGE labs facilities by the consortium of the EU-project OMEGA (www.ict-omega.eu). This system provided 100 Mb/s net data rate. OFDM-based modulation and demodulation, forward error correction, synchronization and a specifically developed Media Access Control (MAC) were implemented on FPGAs. In an area of about 10 m², equipped with 16 LED lamps distributed at the ceiling, four HD-videos were broadcasted simultaneously to four different laptops [51].

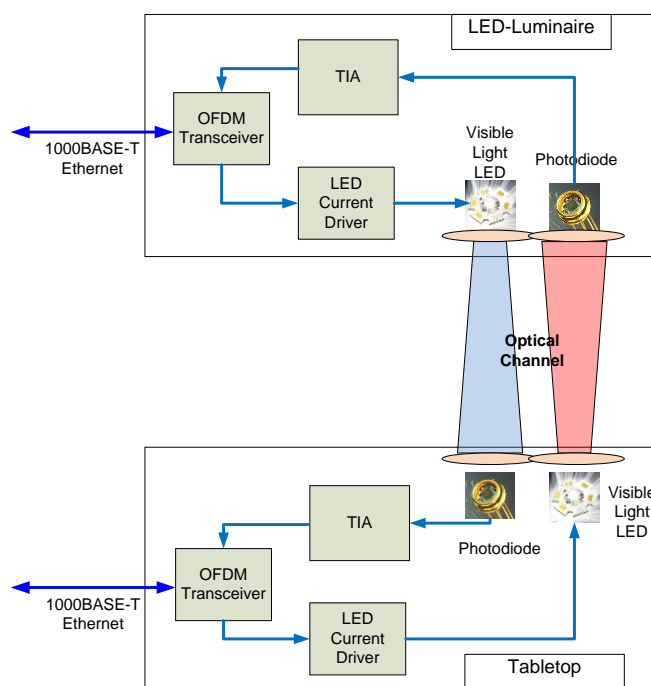


Figure 29: The overall bidirectional real-time line-of-sight (LOS) VLC link.

In order to advance the VLC technology towards future commercial applications, more recently, we developed a bidirectional high-speed real-time VLC system. The idea is presented schematically in Figure 29. Data transmission is based on an optimized, rate-adaptive OFDM modulation and demodulation scheme. The transceivers are equipped with specially designed VLC transmitter and receiver modules. Due to the fact that the VLC channel is based on intensity modulation and direct detection, a real-valued positive waveform is used. Here, DC-biased DMT is applied to obtain a unipolar (positive valued) time domain signal at the transmitter, while potentially remaining negative signal amplitudes are clipped at the expense of an increased error rate. Therefore, the DC-bias and the modulation index need to be chosen carefully at the LED driver. The VLC transmitter is primarily composed of a new LED current driver and an off-the-shelf high-power visible-light LED. The VLC receiver comprises a transimpedance amplifier (TIA) and a commercially available high-speed Si-PIN-photodiode. Our new modules increase the modulation bandwidth from 30 to 180 MHz.

The new transceiver modules have a relatively small form factor (cf. Figure 30), can operate without active cooling and are easily useable. Each transceiver is equipped with an external power supply and 1000BASE-T Ethernet interfaces using standard RJ45 connectors.



Figure 30: Real-time 500 Mb/s VLC system, as shown at a commercial exhibition (right) with the zoom-in of the desk part (bottom left) and the long-range (up to 20 m) version (top left).

A particular advantage of our real-time VLC system is the use of bidirectional, rate-adaptive OFDM transmission enabling a variable throughput with controlled error rate, depending on the quality of the optical communication channel. At a typical working distance of 2 m between the ceiling and the tabletop height, and in a circular spot covering a typical working area of roughly 60 cm in diameter, the system enables a data rate of 200 Mb/s per user. By using narrow-beam optics, we improved the system performance achieving a data rate of 100 Mb/s over 20 m distances. As shown in Figure 31, left, the most important parameter is the light intensity at the receiver, leading to nearly proportional adaptation of the data rate. Thanks to the dynamic rate

control, by reducing the distance, the data rate is steadily increased until the 500 Mb/s peak data rate is reached, (cf. Figure 31, right).

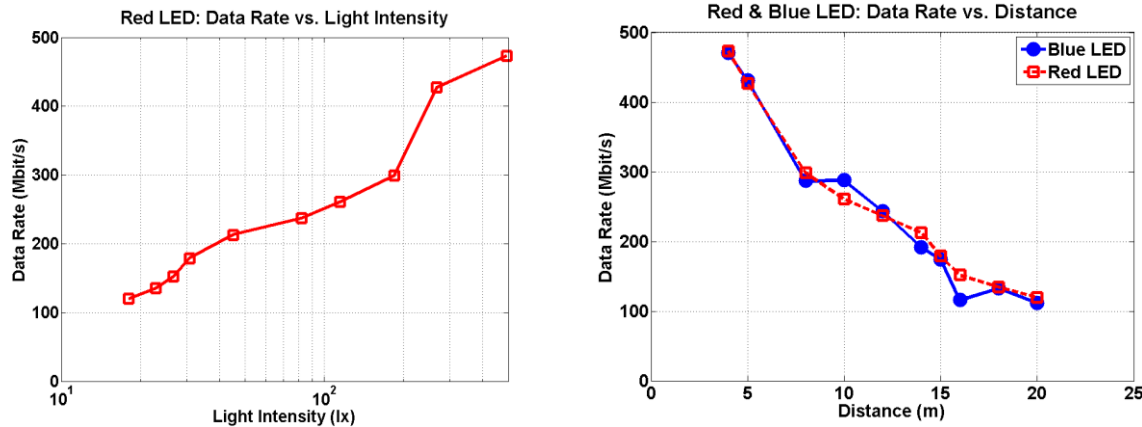


Figure 31: Measurement results for the real-time VLC system. Left: Achieved data rates for the red LED-based transmitter depending on the light intensity measured using a standard photometer at the receiver entity. Right: Measured bidirectional data rates over varying transmission distances demonstrating the virtually colour-independent data transmission.

Our bidirectional VLC experiments demonstrate for the first time that high-speed low-cost optical data transmission can be realized in an indoor setup by using commercially available hardware. We exemplarily used a red and a blue LED source as shown in Figure 30 (top left) for a better visualization of the bidirectional data transmission. As a matter of fact, any other high-power LED could be used as light source instead, independent of its colour. In the near future, we also expect that more powerful OFDM-chips will be available. As our VLC components provide the necessary analogue bandwidth of almost 180 MHz already today, there is an important potential for further increased data rates.

4 Energy Efficiency

Energy efficiency is becoming an ever more critical aspect of assessing network performance, in particular for the access segment, which has been estimated to consume up to 90% of overall telecom network power requirements [52]. Historically, this may be have been due to the preponderance of copper cabling linking homes with the CO; with optical fibre now being ever more extensively deployed for fibre-to-the-curb/cabinet/building/home etc. with its intrinsically lower operating energy requirements, as compared with copper, the overall absolute energy requirement (carbon footprint) of access networks is being reduced.

However, the access network presents additional intrinsic reasons, which make it more difficult to reduce energy consumption e.g. due to its distribution (tree) topology, which makes aggregation (i.e. the ability to combine signals onto a common transmission platform) more difficult and hence makes economies of scale less obvious to achieve. In addition, the heterogeneity of final-drop technologies (i.e. wireless v. fixed, each with their own variations, wireless: 3/4G, WiFi, WiMax, UWB etc., and fixed: FTTH, PON, AON etc.) additionally makes economies of scale more problematic.

That said, there are various techniques that can be exploited to reduce energy consumption, and SODALES does exploit these new technologies to reduce overall carbon footprint. For example, the use of an ARN as a common technology platform for fixed-wireless convergence; statistical multiplexing, in order to maximally and efficiently exploit network resources; scaling of the ARN to optimally allow powering by use of renewable energy sources (wind and solar etc.); locating network intelligence closer to end-users, so that network operating decisions can be made closer to end-users, and hence enable more localized (and end-user optimized) configurations of the access network to be made , and hence enable more energy-efficient operation.

Together, these can be expected to usefully reduce overall access network energy consumption. As the SODALES project develops, we hope to be able to establish some of these energy-saving effects in a more quantitative fashion. However, in advance of this, quantifying an absolute energy efficiency metric, to give a guide as to the optimal target energy efficiency that may be achievable is an important exercise. On the one hand, providing an absolute reference metric (benchmark) is a useful advance from a theoretical and scientific point of view; on the other hand, establishing such a theoretical model for best energy efficiency provides network planners with a tool to optimize the energy consumption of future access networks and to identify the main bottlenecks. Like in a home, where only the optimization of many components altogether leads to a higher energy efficiency (insulation of roof and walls, new windows, renewal of the heating and so on), the same heterogeneous approach may be suitable in the access network. Such a tool and a common metric approach shall include the effects of all relevant components in the access network and will also motivate what may be possible. This will encourage further in-depth research into each component for reaching these theoretical-best energy efficiency values.

In order to establish such a theoretical base-line metric, we need to ascertain some of the intrinsic differences between optical and wireless transmissions systems, in particular, due to their different path attenuations and noise characteristics, so that we can analyse the converged SODALES architecture on a systematic basis. We believe this is the first such converged study of the fundamentals of a fixed-wireless access network.

4.1 Methodology & Benchmarking

One fundamental hypothesis of SODELES is that actively switched network architectures are more energy-efficient than the traditional passive optical networks (PON).

In the traditional PON shown in Figure 32 left, the traffic of many users is aggregated in a passive optical node (being essentially a fibre coupler) and then amplified by an erbium-doped optical fibre amplifier (EDFA) or semiconductor optical amplifier (SOA) for reducing the splitting loss, scaling like $10 \log_{10} N$, which can be huge for large numbers users N.

Statistical multiplexing, which is sometimes also denoted as over-provisioning, is performed at the second aggregation level by using time-division, orthogonal frequency-division or wavelength-division multiple access (TDMA, OFDMA and WDMA, respectively).

Main efforts regarding energy consumption are found in the electric-to-optic conversions at the CPE and at second aggregation levels. Moreover, potentially needed optical amplifiers and the processing of the multiple access protocol by means of TDMA or OFDMA cost significant energy. WDM has a clear advantage in terms of energy efficiency, since optical wavelength are passively combined or split in the AWG. However, the high costs of AWGs increase the CAPEX at the cost of a reduced OPEX.

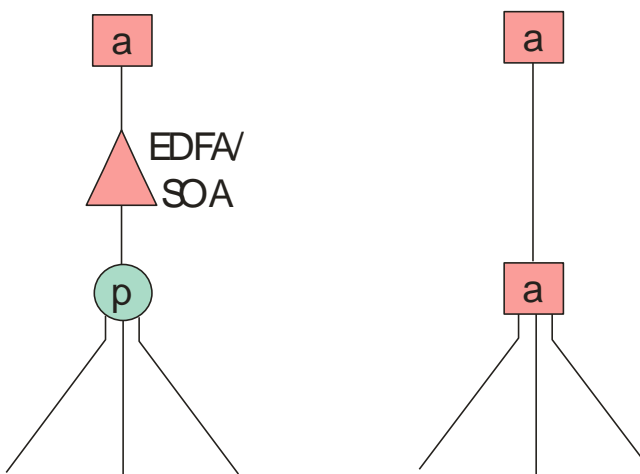


Figure 32: Left: Traditional PON architecture. Right: In an actively switched architecture, the passive node and amplifier is replaced by an ARN in the first aggregation step which is also responsible for the statistical multiplexing.

In the SODELES architecture, the passive node and the (potentially needed) amplifier are replaced by an active remote note (ARN) to which each user is directly connected. From an information-theoretic point of view, this is a two-hop link using decode-and-forward plus statistical multiplexing at the ARN. Since path lengths are shorter, owing to exponential attenuation versus distance, in principal two short hops are more energy efficient than a long one. This effect is relevant in wireless networks, while in optical links it has the consequence that the SNR per user is increased, enabling a higher throughput per user, i.e. the same data can be delivered in a shorter time. The two-hop architecture considered in SODELES offers space for both, increasing the user data rates and reducing the energy consumption.

A second advantage is the statistical multiplexing. It is realized in a standard Ethernet switch, being produced in large numbers of units for computer networks where significant effort is spent by big vendors anyway to reduce energy consumption. In contrast, the statistical multiplexing in a PON is implemented in the OLT in a proprietary manner by telecommunications network vendors delivering also a proprietary ONU. Numbers of units are typically much smaller and optimization of energy efficiency may not be as optimal as in computer networks.

The third advantage of statistical multiplexing is that the data rate in the feeder link from the CO to the ARN is significantly reduced. Firstly, users are not active all the time and aggregation leads to a more continuous traffic in the uplink. Moreover, part of the traffic is local and it can be reflected already at the ARN from one CPE to the other. This holds in particular for future cooperative mobile networks where data and channel state information are shared among the base stations in order to reduce interference. As a consequence, not all data but only the aggregated fraction of data traffic is transported from the ARN to the CO. Hence, lower data rates are needed in the feeder link reducing costs and energy consumption likewise.

On the other hand, there is active processing in the ARN, as opposed to passive combining in the PON, i.e. additional energy has to be spent at first in order to enjoy the reduced energy consumption in the two-hop scenario. Very first practical results show that the ratio between the energy consumption per user port in an Ethernet switch compared to the processing needed in an OLT is in the order of 2/7 [PTI, private information]. These numbers suggest better energy efficiency can be reached by shifting the aggregation task to the lowest aggregation levels and to use standard Ethernet instead of dedicated multiple access protocols as in a PON.

Quantitative benchmarking these two architectures will be conducted in the further progress of the SODALES project. A realistic access network branch, as it is planned for FTTH deployment using a tool available at HHI, will be used as a reference deployment. The different network elements in both architectures are placed into the deployment. Realistic traffics will then be assumed and the energy consumption of each link and each device will be included in the overall study, by using component data available on the market today. The total operational expenditure (OPEX) of the entire access network branch is then obtained. For the wireless traffic, both standard interference-limited networks as well as future cooperative mobile networks will be considered in order to demonstrate the increased effectiveness of the SODALES approach in a future converged fixed-mobile network architecture.

One of the open scientific questions regarding converged fixed and wireless access is to get realistic numbers for the achievable statistical multiplexing ratios in real deployment scenarios, given that a certain quality of experience is ensured for the user. Further research into these multiplexing ratios versus the number of users for which the traffic is aggregated is essential for dimensioning the network appropriately.

Moreover, the optimal multiplexing ratio depends on the underlying traffic models. These models may be different for fixed and wireless access networks since fixed networks feed only the user traffic while there is a significant backhaul overhead associated with cooperatively coordinated wireless networks in the future. Figuring out the right statistical multiplexing ratio is a fundamental work to be done in the SODALES project enabling a proper design of the converged fixed-wireless access network.

Proper dimensioning of components is also related to energy efficiency, since energy consumption depends on the technology and only a small fraction of the overall energy consumption is only proportional to the traffic load. These effects will be taken into account in the system model.

4.1.1 Definition of dB ϵ Absolute Energy Efficiency Metric

It is already well known that the Shannon channel capacity theorem can be simply manipulated to offer the theoretical minimum heat dissipation required to transmit a bit of information. We start from the formula [64]:

$$C = B \log_2 \left(1 + \frac{S}{N} \right) \quad (1a)$$

where C is the channel capacity (in b/s), B is the channel bandwidth (Hz), S is the signal power, and N is the noise power. By considering purely thermal noise as the fundamental noise source in a transmission system, we have the $N=kTB$, where k is the Boltzmann constant, T is the absolute temperature (in kelvins), and B is again the system bandwidth. In the limit of allowing B to increase to infinity, the noise power also tends towards infinity, and we can take advantage of the approximation $\ln(1 + \delta) \rightarrow \delta$ as $\delta \rightarrow 0$. We note that attempting to exploit the maximal (infinite) system spectrum (the full bandwidth as $B \rightarrow \infty$) is analogous to an OFDM or DMT-based communications system, where all bandwidth slots are each maximally exploited with respect to how much data can be transmitted along each frequency slot. In the case as $B \rightarrow \infty$, a slot may offer an exceedingly low data bandwidth; however, we can still exploit whatever minimal data capacity may be available. In the limit as $B \rightarrow \infty$, the Shannon channel capacity equation tends to:

$$C \rightarrow B \cdot \frac{1}{\ln 2} \frac{S}{kTB} \quad (1b)$$

Rearranging the equation (1b), we find that $S/C = kT \ln 2$. The quantity S/C is the quotient of the signal power with the channel capacity, and is equivalent to the number of joules per bit (J/b) of information transmitted across the channel, and is equal to $kT \ln 2$. In other words, as we have already argued from alternative fundamental considerations [58][59], the quantity $kT \ln 2$ represents the minimum amount of energy dissipated by the transfer of information; in addition in ref. [65] we also argue that this energy is essentially irreversibly lost (i.e. it is associated with an increase in entropy of $k \ln 2$ per bit of data.) We have used this minimum energy dissipation per bit to define a decibel-based, absolute energy efficiency metric, $\text{dB}\epsilon$, which offers an objective means to establish the energy efficiency of any information processing system [61]. This is defined as follows:

$$\text{dB}\epsilon = 10 \log_{10} \left(\frac{P/C}{kT \ln 2} \right) \quad (2)$$

where P is the operating power of the information system, C is its data-rate capacity (b/s), and T is its operating temperature. Having established that Shannon's theorem implicitly indicates a minimum energy of $kT \ln 2$ per bit of information for a communications system, in the next section of the paper we derive the Shannon channel capacity equation by analysis of purely classical thermodynamic considerations, starting with Carnot's law of thermodynamic efficiency. In particular, we obtain a more explicit understanding of the nature of the nominal temperature T associated with the noise and communications channel. We additionally derive Shannon's theorem independently of the sources of noise that may exist in a communications system. This allows us to offer an essentially technology-independent insight into the energy, energy-efficiency and noise performances of different telecoms systems, e.g. wireless and fixed (wireline) technologies [66].

4.1.2 Derivation of Shannon Channel Capacity Theorem from Carnot's Law

Carnot's law states that the maximum efficiency η_{\max} by which useful work can be extracted from a heat engine is ultimately determined by the temperature difference between the engine (assumed to take in energy at a high temperature, T_{HI}) and the external environment (at a lower temperature, T_{LO}), such that $\eta_{\max} = 1 - T_{LO}/T_{HI}$. Perfect efficiency can thus only be achieved either for infinitely high temperature, or the environment being at absolute zero – both unphysical concepts. Figure 33(a) indicates the classic textbook schematic diagram of the engine (indicated by a circle), which can be considered as lying between an (infinite) heat reservoir at temperature T_{HI} , and a cooler reservoir at temperature T_{LO} . The useful work extracted from the engine is indicated by the arrow pointing to the right. During operation, the heat engine allows a quantity of energy U to flow out of the high temperature reservoir, such that a maximum fraction of the energy W is output as useful work, and the balance $U-W$ flows into the lower reservoir, with the maximum efficiency therefore given by $\eta_{\max} = W/U$. From an entropy point of view, this is equivalent to the flow of a quantity of entropy $DH = U/T_{HI}$ (i.e. the change in energy in the upper reservoir divided by its temperature) from the hot reservoir to the cold reservoir, where the change in entropy is also given by $DH = (U - W)/T_{LO}$. The ‘useful’ output work (which, by definition, is in itself of 100% useful value) has no entropy associated with it, $DH_W = 0$, i.e. the ‘useful’ output work can be characterised by an infinitely high temperature.

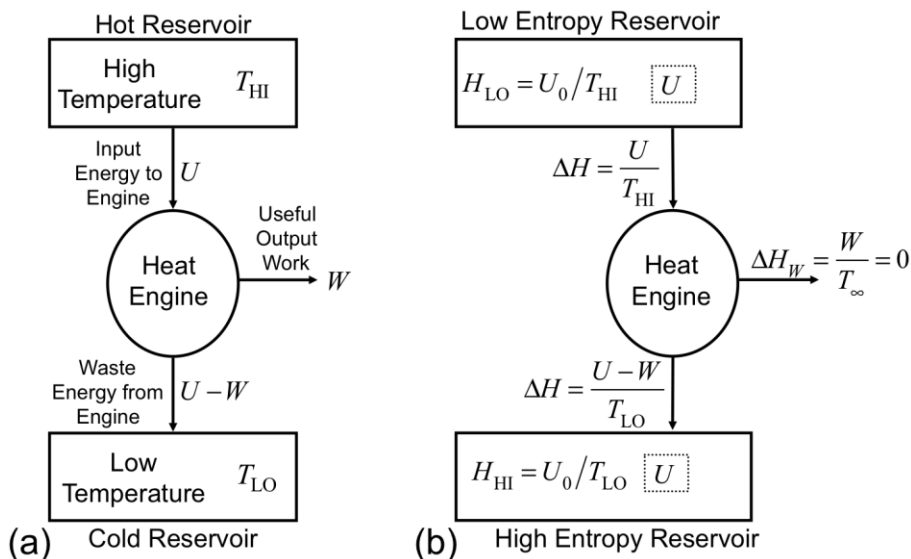


Figure 33: (a) Schematic diagram of a classical thermodynamic heat engine; (b) Equivalent representation showing the entropy states of the reservoirs and the entropy flows.

Conceptually, the heat engine can alternatively be considered as a consisting of an engine placed between a low entropy reservoir (equivalent to the hot reservoir), and a higher entropy reservoir below it (i.e. the cooler reservoir), as indicated in Figure 33(b). In this case, we consider the flow of entropy from the low entropy reservoir to the high entropy reservoir. No entropy flows out via the ‘useful’ output work, since as mentioned above, it has zero entropy associated with it.

It may appear paradoxical that the upper hot reservoir should be characterised by low entropy, since a hot material (e.g. a gaseous form) is generally in a higher state of disorder compared with its colder, generally more ordered counterpart (e.g. a solid). However, the hot reservoir has the greater potential to drive and enable useful work than the cold reservoir. In which case, the entropy of the hot reservoir is necessarily lower than that of the cold reservoir. We can consider the reservoirs to be each filled with an Einstein solid, such that their respective entropy $S_{\text{HI(LO)}}$ is given by:

$$H_{\text{HI(LO)}} = F_{\text{HI(LO)}} k \left[\ln \left(\frac{q_{\text{HI(LO)}}}{F_{\text{HI(LO)}}} \right) + 1 \right] \quad (3)$$

where $F_{\text{HI(LO)}}$ is the number of atoms (oscillators) and $q_{\text{HI(LO)}}$ the number of energy units ε in the reservoir, and k is Boltzmann's constant. At equilibrium, the temperature of each reservoir as defined as $T_{\text{HI(LO)}} = [\partial S / \partial U]^{-1}$, where U is the internal energy. Although the two reservoirs are at different temperatures, we assume that each has the same internal energy $U_0 = F_{\text{HI(LO)}} k T_{\text{HI(LO)}} = q_{\text{HI(LO)}} \varepsilon$. Transferring a quantity of energy U from the top reservoir requires the removal of a quantity F_U of the atoms carrying that energy U . We additionally assume that F_U is sufficiently large to be statistically representative of the hot reservoir, i.e. to be in equilibrium within itself, and share the statistics of the hot reservoir, such that its temperature is also given as $T_{\text{HI}} = U/F_U k$. We assume that the quantities F_U and U are sufficiently small such that $F_U \ll F_{\text{HI}}, F_{\text{LO}}$, and $U \ll U_0$. Considering (1), the reduction in entropy of the hot reservoir is closely given by $\Delta H = F_U k$. For the entropy associated with the sub-partition of atoms $\Delta H = F_U k$ to agree in its own right with (3), requires $F_U \sim q_U$. This has the interesting interpretation that there is approximately one unit of energy ε per atom in the sub-partition of atoms, which implies that they must have similar statistical characteristics to that of a register. After passing through the engine, the ensemble of atoms F_U proceeds to the cool reservoir with an overall energy $U - W$. Again, we assume that for an efficient engine, the statistical state of F_U matches that of the lower reservoir such that $T_{\text{LO}} = (U - W)/F_U k$, with again $\Delta H = F_U k$. We note in passing that for this to be the case, the useful work W must be extracted independent of any of the atoms F_U , (i.e. $F_W = 0$) such that its effective temperature $T_W = W/F_W k$ is infinite, as noted above, and associated entropy from (3) therefore zero, $\Delta H_W = 0$. With the two reservoirs having the same internal energy U_0 and assuming $q_{\text{HI}} \sim q_{\text{LO}}$, we can express the entropy of each of the reservoirs as essentially inversely proportional to their equilibrium temperature. We can also see that the marginal increase in maximum efficiency $d\eta_{\max}$ for a marginal increase in temperature difference dT is simply given by $d\eta_{\max} = dT/T_{\text{HI}}$. We can generalise this further by allowing the high temperature to be variable, e.g. as we allow the temperature difference to vary. In which case the marginal increase in maximum efficiency $d\eta_{\max}$ for a marginal increase in temperature difference dT is now given by $d\eta_{\max} = dT/T$. This is a generalised expression of Carnot's Law, where $T \equiv T_{\text{HI}}$ is the temperature of the higher reservoir at a given instant. For constant T (i.e. as for an infinite capacity reservoir) we immediately recover the traditional expression for Carnot's Law. However, for variable temperature, we integrate the differential equation to get [67]:

$$\int_0^{\eta_{\max}} d\eta_{\max} = \int_{T_{\text{LO}}}^{T_{\text{HI}}} \frac{dT}{T} \Rightarrow \eta_{\max} = \ln\left(\frac{T_{\text{HI}}}{T_{\text{LO}}}\right). \quad (4a)$$

We can again straightforwardly obtain the classical Carnot's law from (4a) for the case when $T_{\text{LO}} \sim T_{\text{HI}}$, i.e. when the temperature difference is small compared with the highest temperature. Thus the maximum efficiency is the logarithm of the quotient of the temperature range; but it can also be expressed using the ratio of the two different entropies, $\eta_{\max} = \ln(S_{\text{HI}}/S_{\text{LO}})$
 $\eta_{\max} = \ln(H_{\text{LO}}/H_{\text{HI}})$.

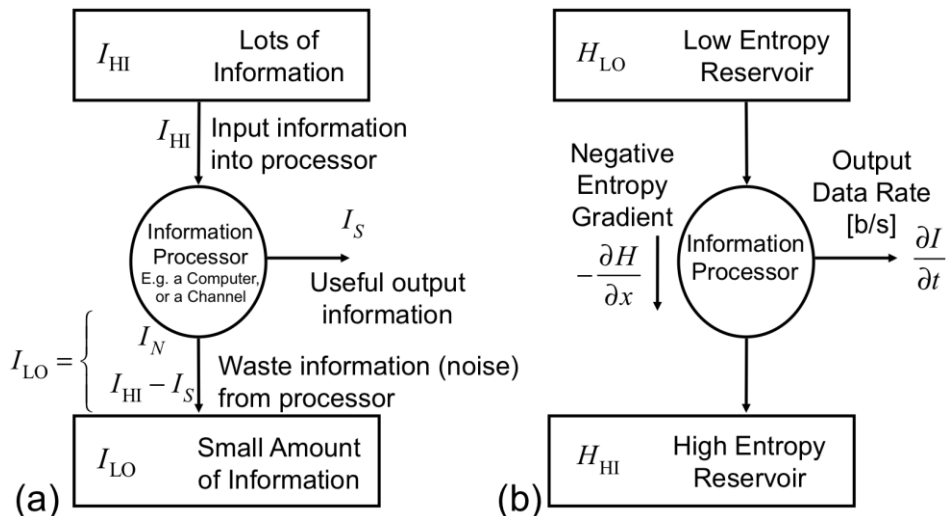


Figure 34: (a) Schematic diagram of entropy flows for an information processor; (b) Equivalent diagram for a Shannon communications system, with channel capacity $C=dI/dt$, and associated (negative) entropy gradient $-dH/dx$.

At this point we remind ourselves of the close relationship between entropy and information. Brillouin considered information to be negative entropy (negentropy [67]), such that a positive quantity of information ΔI is associated with a negative quantity of entropy DH of the same magnitude, such that $DI = -DH$. In which case the high and low entropy reservoirs indicated in Figure 33(b), could also be considered as high and low information (data) storage systems, as shown in Figure 34. Rather than trying to extract useful work from the overall system, we're now interested in extracting useful information from it. Or, in the sense of Shannon's channel capacity theorem, we have a transmitter (containing a high quantity of data, for transmission), with a receiver (which initially doesn't possess the data of interest, i.e. it contains low, or zero information), with a channel in between (the information 'engine' or 'processor') which we hope will 'extract' (i.e. guide) as much of the transmitted information as possible to the receiver. Shannon's channel capacity theorem tells us that the channel cannot achieve this without the introduction of noise, which necessarily makes the process less than 100% efficient. I.e., the signal S being sent can be successfully transmitted to the receiver, but there will always be some energy overhead required to compensate for the effects of noise. In which case, the whole system always has some finite energy loss, such that information cannot be transferred with 100% energy efficiency. In the same way that the maximum efficiency is given by the logarithm of the ratio of the high and low entropies, since information is negative entropy, we can also express the maximum efficiency as the logarithm of the ratio of the high and low information stores in the system:

$$\eta_{\max} = \ln(I_{\text{HI}} / I_{\text{LO}}). \quad (4b)$$

With regard to Figure 39(a), we can see that the ‘information’ input into the channel is the summation of both the ‘useful’ signal S , and noise N , such that:

$$I_{\text{HI}} = S + N. \quad (5a)$$

This brings us to the interesting concept that ‘information’ treats ‘useful’ data and noise equally, i.e. the sum of the ‘useful’ signal and the noise is ‘information’. Superficially this may seem somewhat paradoxical, since we would normally make a clear distinction between ‘useful’ information and noise. However, we note that intrinsically both noise and ‘useful’ information have the same characteristics: Both are necessarily acausal and ‘unexpected’ in nature, i.e. if we could predict what the next signal would be, then by definition it wouldn’t be carrying any new information; likewise, if we could predict what the ‘noise’ would be, then we could cancel it to mitigate its effects, however intrinsic noise is by definition random and non-irreducible. It is also well recognised that a signal containing the greatest information content is one that appears completely random. It then depends on the ‘efficiency’ of the decoding algorithm (i.e. the ‘information processor’) to extract the useful data from that signal! We also note that if we consider the traditional heat engine of Figure 33 (a), we implicitly assume that there is no particular distinction in the energy flowing from the hot reservoir, between the energy which will ultimately output as useful work W , and the energy which flows into the cold reservoir as waste. There is no apriori distinction between the two different energies; likewise, there is no apriori distinction between noise and ‘useful’ information. It just depends on the relative efficiency of the information processor to extract as much ‘useful’ information as possible from the input data. Indeed, two different algorithms (i.e. two different information engines) might each extract a completely different ‘useful’ data set S from the (apriori unknown) input information I_{HI} , but there will always be a residue of unwanted, or waste information I_{LO} , such that the efficiency of the algorithm is always less than 100%. This places information processes on an equal footing with respect to heat engines when considering the 2nd Law of Thermodynamics. The waste information is what we would normally characterise as noise, since as described above, noise has the same properties as information, and by definition any ‘information’ which is undesired, and which cannot be adequately processed by the information engine, is by definition noise. Hence, we can designate the waste information I_{LO} as being equivalent to noise:

$$I_{\text{LO}} = N \quad (5b)$$

Substituting (5a) and (5b) into (4b), we find that the maximum efficiency is given by:

$$h_{\max} = \ln\left(\frac{N + S}{N}\right). \quad (6a)$$

By noting that $\ln 2$ is the unit of 1 bit of information, we can rewrite (6a) as

$$h_{\max} [\text{units of bits/s/Hz}] = \log_2\left(1 + \frac{I_S}{I_N}\right). \quad (6b)$$

Equation (6b) is Shannon’s channel capacity theorem expressed as a spectral efficiency, in units of bits/s/Hz, where of course the quantity s/Hz is dimensionally unity. Hence the maximum capacity in b/s of a channel of bandwidth B is determined by the signal to noise ratio S/N . Conventionally, the SNR is expressed as a power ratio. However, we can straightforwardly

convert between the information quantities of S (or N) and their associated powers using the bandwidth B , and the channel temperature T_{channel} , since $S = BT_{\text{channel}}H_S$, where $H_S = -I_S$, and $N = BT_{\text{channel}}H_N$, where $H_N = -I_N$. Since equation (6b) involves the ratio of the signal and noise quantities, we can straightforwardly express it in traditional Shannon channel capacity form as $h_{\max} [\text{units of bits/s}] = B \log_2 (1 + S/N)$. We note in passing how a positive data rate dI/dt emerging from a communications system implicitly requires a negative entropy gradient, $-dH/dx$, as indicated in Figure 34 (b). In particular, entropy flowing from a low state to a high state (i.e. in accordance with the 2nd Law of Thermodynamics) implies an essentially negative entropy gradient. On the one hand, these differential equations are a direct allusion to the negative difference relationship between entropy and information (i.e. negentropy) as propounded by Brillouin; on the other hand, the combination of these two differential expressions also represents one-half of a pair of Cauchy-Riemann type equations, which together describe a holographic relationship between information and entropy [68].

4.1.3 Inclusion of FEC into Shannon Capacity Theorem

We can also use the Carnot heat-engine model to analyse the efficient transfer of information through a noisy channel, as indicated in Figure 35. In this case, we consider a transmitter placed at position A, with equilibrium temperature T_A , sending a signal of energy U_S to a receiver placed a distance away at B, where the receiver apparatus is equivalent to the Carnot sub-system. We assume the use of forward-error correction (FEC) coding to improve transmission performance, where the FEC coding bits are assumed to have an energy U_{FEC} . We also assume the presence of additive white Gaussian noise (AWGN) in the channel, characterised by a noise temperature T_N , such that in a given time period it is associated with M_N DoF's and an energy U_N . By the time they reach the detector, the signal and coding DoF's $M_S + M_{FEC}$ are mixed with the noise DoF's M_N , such that the temperature at the detector can be characterised by an overall equilibrium temperature T_{HI} , defined by $T_{HI} = [\partial H_U / \partial U]^{-1}$. The total energy reaching the detector is given by $U = U_S + U_{FEC} + U_N$. We assume again that the overall number of DoF's is conserved, $M_U = M_S + M_{FEC} + M_N$, with therefore $U/T_{HI} = U_S/T_A + U_{FEC}/T_A + U_N/T_N$. In which case, the overall temperature at the detector is given by:

$$T_{HI} = \frac{T_A T_N}{\left(1 - \frac{U_N}{U}\right) T_N + \frac{U_N}{U} T_A}. \quad (1)$$

If the noise energy is much greater than transmitter energy, $U_N \gg U_S + U_{FEC}$, then the temperature at the detector tends towards that of the noise source, $T_{HI} \rightarrow T_N$. On the other hand, for dominant transmitter energy $U_S + U_{FEC} \gg U_N$, the detector temperature tends to that of the transmitter, $T_{HI} \rightarrow T_A$. Thus coding techniques with energy U_{FEC} can be used to raise the effective temperature of the detector to that of the transmitter, whilst keeping the signal energy U_S constant. In principle, we want to operate as near to the maximum Carnot efficiency as possible, since that minimises the heat lost to the low-temperature sink reservoir. We assume that it takes a time τ to transmit a signal from A to B. However, at the Carnot efficiency we can only extract information at a low rate, since $M_w \rightarrow 0$, as implied by Figure 33(b), so the amount of information reaching B tends to reduce to zero. As such, in order to actually start extracting information from the communications system we have to operate just below the Carnot maximum efficiency regime. However, as previously indicated, we can operate at an infinitesimally close point,

according to equation 4(a), and then integrate (in effect, over time) in order to actually extract (i.e. receive) the desired data. Thus even though it takes an infinite length of time $t \rightarrow \infty$ we can always transmit all the data that we require. Of course, this conforms with the well-known fact that operating a transmission channel at its Shannon capacity limit, inevitably implies an infinite delay (latency).

In the same way (and similar to our discussion of a calculating machine above), operating at the Carnot efficiency also means that $M_{U-W} \approx M_U$, i.e. almost all the DoF's emerging from the hot reservoir (detector) flow into the cooler sink reservoir at temperature T_{LO} , with the noise and coding DoF's at thermal equilibrium with the sink. Given $M_{U-W} = M_{FEC} + M_N$, we see that the presence of FEC coding DoF's also brings us ever closer to the ideal Carnot condition $M_{U-W} = M_U$, i.e. $M_{FEC} + M_N \ll M_S$. From previous work [59], we have demonstrated that the energy dissipated (i.e. lost to the noise sink) per bit of signal data successfully received at B is given by

$$\frac{U-W}{M_W} = \frac{1+T_W/T_{HI}}{1-T_{LO}/T_{HI}} kT_{LO} \ln 2. \quad (8)$$

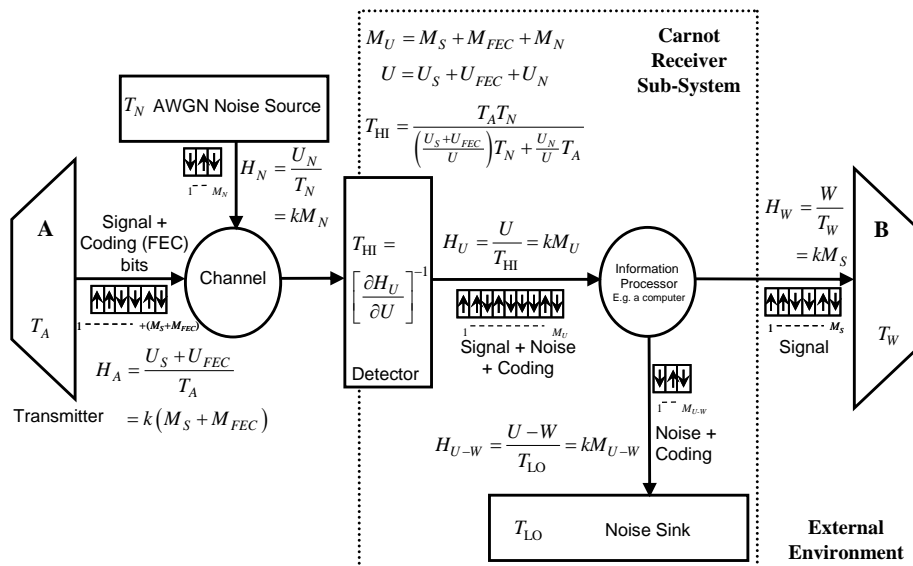


Figure 35: Schematic diagram of an information transmission channel with additive white Gaussian noise (AWGN), characterised using Carnot's law to derive Shannon channel capacity theorem.

With the coding and noise DoF's at thermal equilibrium, the sink energy $U-W = U_{FEC} + U_N$ can be characterised by a 'noise' power $\Delta f k T_{LO}$, where Δf is the bandwidth of the Carnot sub-system receiver. Rearranging (8) using $M_{U-W} = (U-W)/kT_{LO} \ln 2$, and assuming that $T_W \ll T_{HI}$ in order to minimise heat dissipation, we see that the amount of signal information reaching B is proportional to the Carnot efficiency, $M_S = M_{U-W} \eta_{max}$. For notational convenience we assume that the output DoF's are $M_W \equiv M_S$. Thus the maximal amount of signal information reaching B depends on the temperature difference between the detector and heat sink. For a marginal temperature difference dT between them, with the detector temperature $T = T_{LO} + dT$ and that of the sink T_{LO} , then the marginal Carnot efficiency is given by $d\eta_{max} = dT/T$. In this case, the marginal amount of

signal information reaching B is $dM_S = M_{U-W} d\eta_{\max}$. Assigning a power S to the signal information reaching B, and integrating over the transmission time τ we have $W = U_S = tS$. Likewise, during that time τ , we also assume that the integrated waste (sink) energy is given by $\tau\Delta f k T_{\text{LO}} = U - W = M_{U-W} k T_{\text{LO}} \ln 2$, i.e. the noise and coding DoF's are also alternatively given by $M_{U-W} = \tau\Delta f / \ln 2$. The coding and channel noise powers are therefore respectively given by $U_{\text{FEC}} = \tau P_{\text{FEC}}$ and $U_N = tN$. Hence, the marginal amount of signal information reaching B in the time τ due to a marginal temperature difference is $dM_S \ln 2 = \tau\Delta f dT/T$. Increasing the temperature difference between the detector and heat sink therefore allows us to increase the quantity of signal information reaching B. Increasing the temperature of the detector can be achieved either by increasing the signal power or adding extra coding bits to the signal, e.g. as indicated in (5). Summing (i.e. integrating) the marginal increases in information as we increase the temperature of the detector from T_{LO} to T_{HI} yields:

$$\int_0^{M_S} dM_S = \frac{\tau\Delta f}{\ln 2} \int_{T_{\text{LO}}}^{T_{\text{HI}}} \frac{dT}{T} = \frac{\tau\Delta f}{\ln 2} \ln\left(\frac{T_{\text{HI}}}{T_{\text{LO}}}\right). \quad (9)$$

Due to its inherent stochastic nature, the AWGN noise from the channel cannot be cooled lower than T_N , which means that the fundamental lower temperature of the heat sink is $T_{\text{LO}} \geq T_N$. Assuming perfect coding, which allows us to reach that lower temperature limit, then the ratio T_{HI}/T_N can be expressed within (9) as:

$$M_S/t = Df \left[\log_2 \left(1 + \frac{S + P_{\text{FEC}}}{N} \right) - \log_2 \left(1 + \frac{M_S + M_{\text{FEC}}}{M_N} \right) \right]. \quad (10)$$

Here, we have used (from Figure 35) the fact that $T_{\text{HI}} = U/kM_U$ and that $T_{\text{LO}} = U_N/kM_N$, where $U = (S + P_{\text{FEC}} + N)t$, and $U_N = Nt$. Equation (10) is a generalised expression for the maximum channel capacity, based not just on the powers but also on the DoF's of the signal, coding and noise. If we assume additive, white Gaussian noise (AWGN), we can assume that the noise DoF's are much greater in number than the signal and coding DoF's, $M_N \ll M_S + M_{\text{FEC}}$, such that we can neglect the second logarithm term in (10), and we can find that the signal data rate M_S/τ approaches the Shannon capacity C [b/s] of the channel, given by:

$$C = Df \log_2 \left(1 + \frac{P_{\text{Tx}}}{N} \right), \quad (11)$$

where $P_{\text{Tx}} = S + P_{\text{FEC}}$ is the total transmitted power. Indeed, we see that AWGN is probably the most benign type of noise in terms of its impact on the capacity of a communications channel, with just the average power of the noise N appearing in the classical Shannon capacity equation. However, as can be seen from equation (10), where the DoF's of the noise M_N are not high, then the channel capacity is reduced further. For example, possibly the most disruptive type of noise is impulsive in nature. In this case, the number of noise DoF's is just $M_N = 1$; a noise impulse is either present or not. In this extreme case, the second logarithmic term on the RHS of equ.(10) is maximal, and the channel capacity therefore significantly reduced. Indeed, in the presence of impulsive noise, it appears that a low complexity modulation format (i.e. binary on-off keying, OOK) where $M_S = M_{\text{FEC}} = 1$ will enjoy the highest channel capacity, with more complex

modulation formats, e.g. the various QAMs and multi-level formats, theoretically exhibiting an essentially lower throughput data rate in the presence of impulsive noise. Hence, the FEC coding brings us ever closer to the theoretical Shannon capacity limit.

Using $P_N = \Delta f k T_N$, and letting the system bandwidth increase indefinitely, we find that the energy per bit of transmitted information is $P_{Tx}/C = k T_N \ln 2$. We note that whilst the signal DoF's M_S reaching B represent the information signal that we wish to transmit to B, the DoF's M_{U-W} entering the cold sink reservoir are DoF's extraneous to the (useful) signal DoF's, and at the lowest sink temperature possible $T_{LO} = T_N$, are analogous to noise. The heat lost to the cold sink reservoir is therefore equivalent to noise energy, and must be dissipated. Hence, the minimum energy dissipated as noise per bit of signal information transferred is indeed $k T_N \ln 2$. The lower the noise temperature, the less energy is dissipated per signal bit of information. We note that this minimum energy dissipation is also only asymptotically achieved as the temperature of the detector (and hence additionally the transmitter at A) tends to infinity, $T_{HI} \rightarrow \infty$, according to equation (8). Thus energy dissipation in information transfer is inherently due to the presence of noise (i.e. a finite noise temperature) in the channel. If there were no noise, then no energy need be dissipated to transfer information. However, a noiseless channel is physically impossible, as we have previously discussed [65].

4.1.4 Application of Theory to Wireless & Wireline Communications Systems

We now briefly apply our theoretical results to the following four communications systems: i) optical direct-detection; ii) coherent optical; iii) radio or wireless; iv) electrical. In particular, we want to characterise how the associated noise temperature T_N for each of the systems relates to each other, and the resulting impact on the theoretical minimum energy required to transmit a bit of information for each system. It is well known that a coherent optical system enjoys a 3dB noise figure advantage over its direct-detection equivalent, which means that the effective noise temperature $T_N|_{coh}$ is half that of the direct-detection system, $T_N|_{coh} = 0.5 T_N|_{dd}$. Similarly, as can be seen from the equation (10), the employment of advanced modulation formats (e.g. as seen in both wireless and coherent optical communications) requires additional DoF's, M_S and M_{FEC} .

Table 1: Noise temperature Technology co-efficient factors

Technology	Co-efficient	Value
Coding Efficiency	β_0	$\frac{1 + T_W/T_{HI}}{1 - T_{LO}/T_{HI}}$ ^{3.1}
Coherent detection	β_1	0.5
Multi-level coding	β_2	$\log_2 L$
Quadrature modulation	β_3	2

This means that when the energy-per-bit is calculated from equ.(10), the resulting increase in energy per bit can be encapsulated into an equivalent higher noise temperature. In this case, the increase in equivalent temperature as compared to a simple OOK direct detection is a factor

$\log_2 L$, where L is the number of levels in a L -ary modulation scheme; similarly, depending on whether quadrature modulation is employed, this also requires a doubling of the number of DoFs, such that the energy per bit increases by a factor 2. As such, we can define the equivalent noise temperature for a particular communications technology as

$$T_N = b_0 b_1 b_2 b_3 T_{LO} \quad (12)$$

where the co-efficient factors in the set $\{b\}$ take on the values according to the type of communications technology being employed in Table I. When a particular technology is not being employed, then the value of the particular β co-efficient associated defaults to unity. We note in equation (12) that the temperature factor T_{LO} is used as the base-line for the noise temperature T_N , where the efficiency of the coding and/or communications technology determines the temperatures T_W , T_{HI} , and T_{LO} and hence the co-efficient b_0 according to equation (8).

4.2 CO-ARN Technologies

The interconnection between the Central Office (CO) and ARNs is faced in SODELES with the aim of offering the highest possible bandwidth at the lowest cost while providing essential features for Open Access operation.

One can distinguish between optical transport and link protocols, being both involved in the interconnection between the CO and the ARN. In terms of optical transport and layer-2 connectivity, three approaches are foreseen in SODELES. Those are:

- OTN
- Carrier Ethernet
- MPLS-TP

This section provides an overview analysis of the energy efficiency of these three technologies in order to provide the best option to SODELES.

4.2.1 Optical Transport Network

OTN is designed to provide support for optical networking using wavelength-division multiplexing (WDM) at high data rates. ITU-T Recommendation G.709 is commonly called Optical Transport Network (OTN) (also called digital wrapper technology or optical channel wrapper) and provides datarates that range from 2.5 Gb/s to 100 Gb/s.

OTN is a technology initially developed for core networks, which offers monitoring and segmentation at the optical level. It can be a good candidate for SODELES, as supports multiple traffic encapsulation methods and provides support for both, packet and TDM networks.

However, the cost of OTN is substantially higher than to deploy a Carrier Ethernet or MPLS-TP implementation

4.3 Local v. Remote Powering

Remote powering is a concept for distributing DC power over existing twisted pairs up to 10 km. The concept is typically for use in broadband applications, where telecom equipment is located close to the end-user and requires power. What makes remote powering attractive is the independence from local power utilities and centralized back-up systems (batteries). The system consists of a Central Office Remote Power System and a remote-end converter.

However, at present, the use of green energies to generate electricity at the ARN side is foreseen as a better option to optimize the efficiency of the system.

The options are described below and include:

- Wind and solar
- Fuel cells
- Pico Hydro

4.3.1 Wind and Solar

Solar and wind power have progressed in recent years with costs steadily falling. The point is being reached where they can be considered as supplementary or even the primary power source for cell sites in difficult locations. As the cost of wind and solar technology continues to fall, and the cost and scarcity of fossil fuels increase, solar and other renewable energies will become increasingly cost effective compared with more conventional power sources. While wind and solar are independent power sources, here they are combined to highlight how Motorola is combining the two sources to provide reliable energy to base stations.

Solar power is generated using the photovoltaic properties of semi-conductors to convert light energy into electricity. Manufacturing costs for solar cells have been declining by 3-5% per year in recent years, leading to growth capped only by silicon supply issues. For wind power, a wind turbine attached to an electrical generator converts wind power to electrical energy. Globally, wind power production quadrupled from 2000 to 2006. It accounts for 20% of electricity use in Denmark, 9% in Spain, and 7% in Germany.



Figure 36: Wind and solar power generation equipment

The global adoption of wind and solar as commercially viable technologies, together with the falling costs and growing reliability of the technologies, make them cost effective technologies to adapt to a telecommunications environment.

4.3.2 Fuel Cells

Fuel cells are emerging as a strong alternative power source candidate. The technology has matured in recent years and has many benefits compared to generators, such as fuel efficiency, climate resistance, reliable start-up, and being very compact (e.g. fitting in a 19" rack). Their silent operation means there will be no indication that a power source is operating on the cell site, reducing the likelihood of theft. Having reached volume manufacturing and with prices falling, they will challenge conventional engine driven generators in terms of cost and reliability.



Figure 37: Fuel cell generation experiment

Fuel cells operate by converting a fuel, such as hydrogen, into electricity without combustion. There are several types of fuel cells, of which the most promising for telecommunications is the Proton Exchange Membrane Fuel Cell (PEMFC). The PEMFC operates at low temperatures, and runs at 40-60% efficiency.

4.3.3 Pico Hydro

The term pico hydro refers to very small hydro systems. There is a large potential market for pico hydro due to the fact that:

- Small water flows are required;
- Small communities in the developing world are often not linked to a power grid;
- Locally manufactured pico hydro systems have lower long term costs per kilowatt than;
- solar, wind, or diesel systems;
- Hydro systems provide constant energy during times of normal rainfall.

Today, the primary use of pico hydro is for lighting and basic electrical needs in remote areas. However, areas with high rainfall, steep flowing streams and rivers provide an ideal source of power for wireless communication network base stations, allowing the low cost, low maintenance deployment of wireless communications to emerging markets.

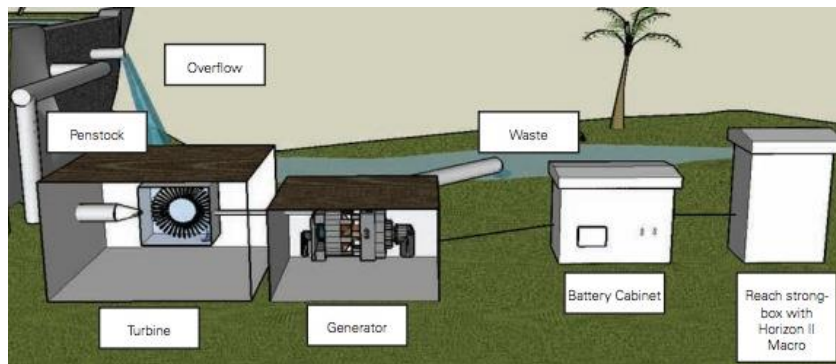


Figure 38: Pico Hydro power generation systems

One of the problems of this system is that typically, antenna sites tend to be at high level points, while pico hydro systems take advantage of ramps to generate energy at the lowest possible point.

5 Service Quality Analysis

The emergence of bandwidth greedy applications is constantly pushing the need to deploy large capacity optical fibre at the access networks. Optical access technologies support huge bandwidth capacity but are ‘costly to deploy to each user’s premises’ [52]. Furthermore, the existence of large, increasing, mobile users creates market opportunities. Consequently, there is growing interest by carriers and service providers to exploit the benefits of both wired and wireless technologies. Wireless services are easier to deploy and offer the benefits of flexibility and cost [70]. This growing interest attracts advancement toward convergent network architecture capable of delivering heterogeneous services to serve different categories of users. Hybrid optical-wireless networks are poised to provide such converged network and offer both wired and wireless broadband services to the end users. Emergent hybrid networks deploy wireless network to utilize available bandwidth, provided by existing optical reach, in generating higher revenue.

Despite the opportunities, converge network architecture present other challenges. Example is the need to properly manage the heterogeneous devices in order to achieve full efficiency. Recent research [52][71][72][73] suggests the integration of active remote node (ARN) close to the service drop point. ARN in hybrid optical wireless networks (FiWi) offers the flexibility to deploy traffic management functionalities for higher user experience and better performance [74]. Using ARN ensures that the variation [70][75] in traffic request at various times of day (e.g. due to mobility, and differentiated services) and at different service areas are exploited to offer dynamic configuration of access network elements.

In this chapter we present a dynamic software defined ARN suitable for next generation high capacity access networks. We specifically utilize the concept of software-defined network to build time series user traffic statistics model, which is then used by management function to dynamically allocate traffic on the backhaul link of access network. The rest of the chapter is organized as follows. The next section presents an overview of access network, section 5.2 presents our proposed strategies, and section 5.3 presents some initial simulation results.

5.1 Overview of Higher Performance in Converged Access Networks

Optical networking emerged to connect long distance communication nodes. Long haul optical networks have been gradually extended to provide optical at access level in different types including passive optical access network including Fibre-to-the-Home (FTTH), Fibre-to-the-Building (FTTB), FTTCurb (FTTC) and FTTCabinet (FTTCab) [10]. Two widely access networks are TDMA-PON and WDM-PON. TDMA-PON provides time-shared access to switching resources. As the requirements to support new applications and architectures surge, Ethernet based PONs gain popularity due to, in part, their support for

Various proposals to integrate optical and wireless are available in the literature. Proposal in [71] implements a resilient wireless-optical broadband access network where users connect to wireless backhaul using ONU and users access any available ONU by forming a multi-hop mesh network. One approach to achieve reconfigurable optical access network is to deploy router in form of splitter (AWG). In [76] this is achieved by deploying tuneable devices at the PON and

tuning the required ONU at the access end to one of these groups in event of overload at the PON primary serving area. The allocation and scheduling are implemented at the central office equipped with a bandwidth monitor that constantly monitors the downstream traffic buffer of each OLT. An obvious challenge is the reconfiguration delays for bursty and unstable traffic. This frequent reconfiguration significantly increases the delay experience by packets.

In [77] the wireless is deployed as front end for large capacity optical network. The proposal adopts dynamic ONU selection enabled by remote node (RN) to achieve effective bandwidth allocation. The proposed RN facilitates routing and attempts to minimized power consumption of previous proposal [78] with the design of $2 \times \omega$ AWG and $n \times 1$ passive combiners; where ω and n are the numbers of wavelengths and ONUs respectively. In [73] intelligent RN is equipped with lookup and layer 2 forwarding logic to reduce OLT to ONU traffic in integrated wireless optical front end access network. The proposed RN implements snooping to filter network traffic and reduce the traffic load at the OLT. This type of fiber-wireless integration is loopback in nature where ONUs communicates directly without the need for OLT. More advanced quality of services (QOS) functionalities are achieved in [72] by deploying two RNs and using unique physical logical link identity to reduce the RN lookup delay.

In [79] is proposed the direct transport of wireless signals over fibre. The research work describes the technique of joint processing at Central Office (CO) where all computations and allocation of bandwidth are carried out at CO thereby reducing the functional requirements at RN.

The proposal in [71] collates user traffic statistics at various times of the day and utilize the variation in the user request to achieve an energy aware routing that shut down ONUs in periods where traffic load is less than certain threshold. Another traffic based dynamic hybrid network is reported in [52].

All the aforementioned proposals for optical and wireless integration assume separate ARN and ONT. However, in the novel approach of SODALES ARN architecture the ONT is considered as part of the ARN, and terminated with the 120G Ethernet switch. This enables the architecture the flexibility to choose final-drop technologies: either wired (fibre-optical, FTTH) or wireless (radio/mm-wave/optical) to the residential home, and likewise convergence with mobile communications.

Connectivity at the last mile has been traditionally provided by passive access network. Three categories of service areas exist: residential (Res), Medium-sized Enterprise (SME), and the combination of these two. The residential (Res) is characterized with large number of users requiring broadband services for multimedia and data. Recent research [70][75] identified the unique feature of the users in this category to generate large traffic during the night and below average during the daytime.

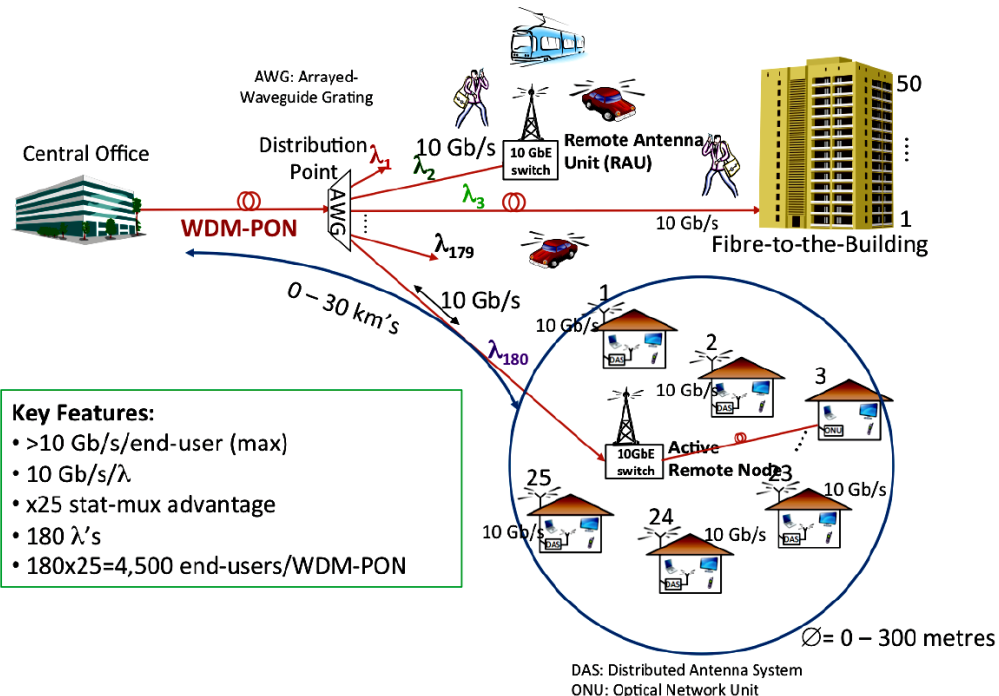


Figure 39: Demonstrating the user and resource interactions in point-to-multipoint access network

5.2 Traffic Patterns

Residential broadband traffic patterns varies considerably in terms of usage and application types [70][75]. The IEEE 802.16 [80] accepted the ON/OFF wireless traffic model [81] as reliable for simulations of wireless networks. The model adopts superposition of various Poisson distributions to produce a batch Markovian arrival process (BMAP). Recent research [75] on residential traffic pattern indicates varying traffic load at different times of the day for Res and SME. If we assume that the residential users in figure 1 request their traffic content from the internet, then we can effectively model the popularity of accessing particular broadband service using Bimodal Zipf; session arrivals using exponential for short time-scales, time-of-day and time-zone using correlated behaviour; and finally session durations using heavy-tailed [82].

5.3 Flow Scheduling for SODEAS Network

The SODEAS ARN enabled access network architecture is depicted in Figure 39 and provides N wavelengths each carrying 10 Gb/s. SODEAS envision the research into access network having advanced control and management plane with open-access and multi-operator functionalities. The initial proposal of SODEAS considers the ARN comprise of 120G switching fabric and connected to the CO using 2 wavelengths. In this model, we have the ARN consisting of a 120G=3×40G Ethernet switch chassis, where the first 40G rack has 4 output ports of 10G capacity each, connected respectively to the RBS and 3 SMEs. For these users, there is no contention or statistical multiplexing. The other two 40G racks each have 48 output ports, each offering a maximum 1 Gb/s bandwidth pipe. In Figure 39, a total of 20 Gb/s (equal to 2×λ @10 Gb/s/λ) light paths are used between the ARN and the CO. We call these two wavelengths high and low priority wavelength and denote them as λ_H and λ_L respectively. Apart from this, the XG-

PON function is conventional, with an intermediate AWG wavelength-routing lightpaths to other ARNs, or even allowing dedicated wavelengths to be directly routed to a 10G ONT located at a RBS or SME business premises.

In this arrangement, three scenarios are considered:

- All λ_H and λ_L are available for the 96 Res users. This scenario is common where ARN is located in a purely residential area, without any SME or industry requirements
- RBS and SME are allocated 30% (or equivalent fraction) of λ_L and the remaining 70% (or equivalent) is available for the 96 Res as a super link.
- All RBS, SME, and Res contend for the λ_H and λ_L wavelengths.

The flexibility offered here means that differentiated services, varying bandwidths, and differing end-user densities can be efficiently catered for. The proposed optical wireless access network architecture is depicted in Figure 40 and we assume the following:

- 2 wavelengths connect the ARN and the CO;
- Users vary in their traffic request;
- A node at the ARN implements basic software define logic which feeds back statistics to the central office;
- Wavelengths are regarded as limited and scarce resources;
- Non-negligible time is required to create and release optical path from source to destination.

Given the requirements described above, we can formulate a problem statement for the 2 available Lambdas connecting ARN and CO.

5.3.1 Problem Statement

Given an optical link with 2 λ connecting the large residential users U attached to the intelligent ARN, the fundamental requirement is to provide access network connectivity from ARN to CO for $U >> 2\lambda$ based on each $u \in U$ request r . In other words, we seek to map $U(r) \rightarrow 2\lambda(c)$ where c is the capacity of each λ .

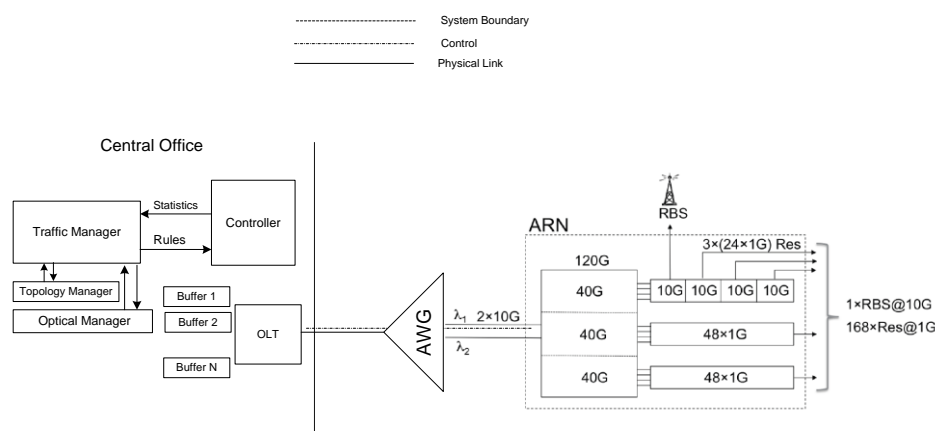


Figure 40: SODELES access network architecture.

5.3.2 Software-Defined Networking for ARN

A key component of our proposed architecture is a centralized software defined network controller (SDNC). SDNC logically controls the behaviour of the entire access network. The SDNC implements basic control protocol logic and enable the storage of traffic statistics and devices information. Communication between network nodes and controller is through dedicated channel. For simplicity, we assume such communication does not contribute significantly to the network traffic.

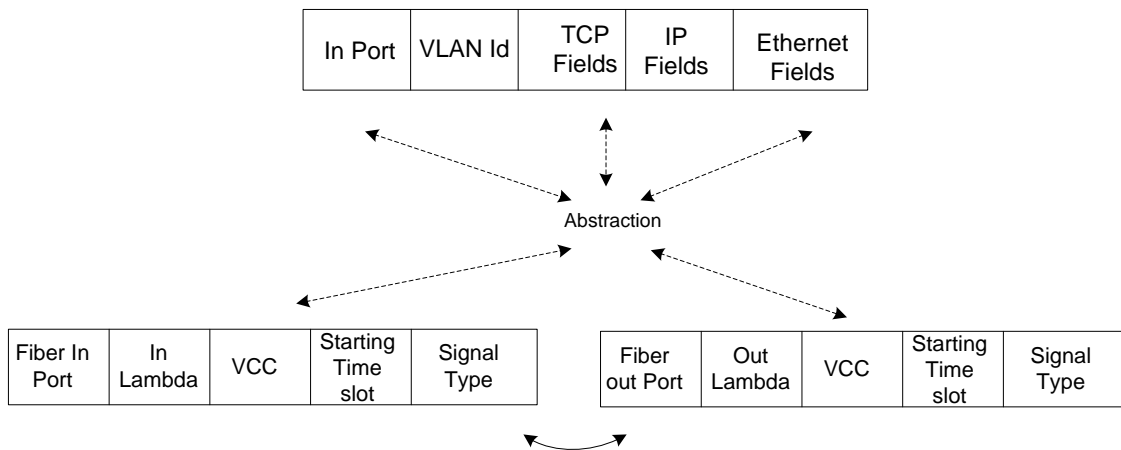


Figure 41: Mapping packet flow headers to optical flow headers

The SDNC maintain abstraction from the headers in the packet fields to the optical header (OP_HEADER). This way both entries in the Ethernet packet and transport network elements are viewed as flow entries. The abstraction and subsequent mapping is significant in eliminating the technological differences between circuit flows and packet flows, thereby leading to true convergence.

The controller in Figure 41 queries aggregate flow statistics from gigabit switches at the ARN. The switches respond with statistical flow information including table Id, flow count, flow descriptors, out port, in port, packet count, and total byte count. Using SDN controller in a network enables dynamic reconfiguration of communication devices.

5.3.3 Topology Manager

In our work we integrate a topology manager to provide services to the controller. The topology managers re-compute topology in event of changes in links and node status. New nodes joining the network are also considered in the graph and this triggers re-computation of the traffic graph. This way the controller is aware of the overall network topology making it easy to manipulate forwarding tables with appropriate actions. Every time a packet arrives at SDN enabled Switch, the switch search the flow action table in the switch. The action flow table list flow characteristics and matching action. If there is a policy relating to the new packet an appropriate action is taken on the packet. Action can be to forward the flow to the appropriate wireless access device or to the AWG using choosing wavelength. If there is no matching action for this flow it is encapsulated and send to the controller. Appropriate action is created for the flow and the action tables of the switches updated. Next time the same flow arrive at a switch the action is then applied.

5.3.4 Traffic Manager

We formulate the architecture (Figure 40) for dynamic traffic management in hybrid optical and wireless access network, which also depicts the functional structure of our proposed architecture. It comprises a controller, Traffic Manager, and optical manager.

- Network nodes send traffic flow statistics updates to CO.
- A traffic manager then generates a traffic matrix with source, destination, and weight identifying each entry.
- A traffic graph is generated with vertices and edges denoting nodes and traffic contribution.
- Selection of suitable flows for offload to one of the wavelengths.

For our model, we model a flows traffic network as a weighted and non-zero graph, $G(V, E)$, consisting of paths connecting $X \in V$ and $Y \in V$. Data travel between vertices V by way of the edges E . X is regarded as the input and Y the output. Traffic statistics from each flow is a 5-tuple (u, v, ω, p , and m). For packet size - ω , source - u , destination - v , port type - p , and media (wireless or wired) m . The traffic manager treats all traffic from node u to node v as $F_{u, v}$. It maintains traffic statistics as $n \times n$ matrix such that:

$$A_G = [a_{u,v}] \begin{cases} a_{u,v} = \omega_{u,v} & \text{if } u \neq v \\ a_{u,v} = 0 & \text{otherwise} \end{cases} \quad (13)$$

with entries $a_{u, v}$ defined by an undirected graph $g = \{V; E; \omega\}$, for $u, v \in V$, such that $\omega : V(g) * V(g) \rightarrow \mathbb{R}^+$, satisfying $\omega(u, v) > 0$, $\omega = F_{u, v} = F_{v, u}$. We simplify our model as undirected traffic graph. At any time intervals t and t' , the traffic matrix generates graphs g and g' respectively. We compute traffic threshold value h_T as a function of packet network traffic load and link capacity. h_T is the parameter that guarantee flow feasibility. We say that a network is feasible if there exists a flow $F_i(u, v) : V(g) * V(g') \rightarrow \mathbb{R}^+$ satisfying $\sum F_i(u, v) \leq C(u, v)$ where $C(u, v)$ denotes the capacity available. Four stages are involved in our proposed dynamic traffic scheduling.

The first step is traffic change detection. This first step avoids the need to compute bottleneck coefficient every time as this is computationally expensive and classified under categories of NP hard problems [84].

5.3.4.1 Traffic Change Detection

Consider graphs g, g' and g', g with set of edge weights ω, ω' and ω, ω' . The relative amount of change over period $\nabla t = |t - t'|$ between edges is given by $d(g, g')$. For any non-zero weights and $u, v \in V$, the traffic change between u and v as the traffic graph evolve from g to g' is thus:

$$|\omega(u, v) - \omega'(u, v)| \quad (14)$$

Clearly $\max(\omega(u, v), \omega'(u, v)) \geq |\omega(u, v) - \omega'(u, v)|$. And the transformation:

$$d(g, g') = \hat{\bigtriangleup} \frac{|\omega(u, v) - \omega'(u, v)|}{\max(\omega(u, v), \omega'(u, v))} \quad (15)$$

normalizes the traffic change over all the edge sets in V. Once a significant change is detected in the graph, the next stage is started.

5.3.4.2 Estimating the Bottleneck Coefficient

We adopt Laplace implementation of the Cheeger constant [84] h_T to investigate existence of possible bottleneck in λ_L . This measures the need to offload packets in λ_L to λ_H . We chose Cheeger constant mainly due to existence of algebraic relationship with proposed Laplacian model adopted in this paper. h_T is estimated to give a measure of the level of bottleneck in a network flow traffic when modelled as a graph comprising source and destination sets. We particularly use the weighted model of h_T . Using the relationship presented in [86] to make provision for traffic edge weight we estimate h_T , as $h_T = \inf(h)$ where h is defined as:

$$h = \frac{|C(S,D)|}{\max_k \left(\sum_{u \in S} d_u, \sum_{v \in D} d_v \right)} \quad (16)$$

Where $C(S,D)$ is capacity set of edges with vertex incident at S. S:set of source nodes, D:set of destination nodes, d_u is the traffic with source incidence at u and not at v, and d_v is the traffic with source incidence at v and not at u. Two cases exists to describe h_T [84] :

- $h_T < 1$ bottleneck exists
- $h_T \geq 1$ feasible flow exists

Estimating h_T has been shown [86][84] to be NP-Hard problem since the computation, by definition, can take prohibitive exponential time for small number of vertices. The approach is to obtain an estimate after considerable traffic change is reported in the first stage. The existence of bottleneck triggers the investigation of exact region of change.

5.3.4.3 Identifying Dominant Traffic Region

To detect the contribution by flows to the experienced changes in our graph g and g^l , we use the concept of graph Laplace Spectra which measures both the weight and the logical connectivity dominance of a flow. This approach is similar to transport flow measurements introduced in enterprise networks and applied to compute relative changes [85] in real traffic networks such as vehicle traffic network.

LSG measures both flow contribution and logical flow connectivity. The premise of considering logical flow connectivity is the strong relationship between flow diversity and sustainability over time. Under this a flow with many related flows is expected to last longer making it suitable for optical switching. To compute specific region of change we first define weighted Laplace matrix as:

$$L(u, v) = \begin{cases} d_v - \omega(u, v) & \text{if } u = v \\ -\omega(u, v) & \text{if } u \text{ and } v \text{ are adjacent} \\ 0 & \text{otherwise} \end{cases} \quad (17)$$

Where $\ell = D^{-1}LD^{-1}$ and $dv = D^{-1}(v, v) = 0$ in the relation. ℓ is the Laplace of graph g. The eigenvalues of the Laplace graph has been shown in [84][87] to be a good and stable indicator of changes in a graph. A Laplace of graph g and spectral index $\rho(Ag) = \lambda_0, \lambda_1, \dots, \lambda_n$ is defined as $\ell_g = D_g - A_g$. Where D_g and A_g are the diagonal matrix and weighted adjacency matrix of g respectively. The Laplace of g is otherwise stated as:

$$\ell(u, v) = \begin{cases} 1 - \frac{\omega(u, v)}{d_v} & \text{if } u = v \\ -\frac{\omega(u, v)}{\sqrt{d_v d_u}} & \text{if } u \text{ and } v \text{ are adjacent} \\ 0 & \text{otherwise} \end{cases} \quad (18)$$

Let the spectral matrix of g and g^l be given by $\rho(Ag) = \lambda_0, \lambda_1, \dots, \lambda_n$ and $\rho(Ag^l) = \mu_0, \mu_1, \dots, \mu_n$. n is the number of nodes in the graph at point of computation. And $\lambda_0, \lambda_1, \dots, \lambda_n$ is the spectrum of the graph. We expect the eigenvalues to change systematically if the graph links and their weights show systematic change. The difference between the spectra provides us with a distance measure between two graphs g and g^l . We normalize the differences as in [84][88] to obtain

$$d(g, g^l) = \sqrt{\frac{\sum_{i=1}^k (\lambda_i - \mu_i)^2}{\min(\sum_i \lambda_i^2, \sum_i \mu_i^2)}} \quad (19)$$

By considering sub graph $g(u, v)$ such that $u, v \in E$ in Equation (19) we obtain the Laplace traffic distance as:

$$d(u, v) = \sqrt{\frac{\sum_{i=1}^k (\lambda_i(u, v) - \mu_i(u, v))^2}{\min(\omega(u, v), \omega^l(u, v))}} \quad (20)$$

Equation (20) gives specific Laplacian spectral distance for a flow identified by nodes u and v . $k=20$ have been shown in [87] to be a good value for investigating significant changes in graphs.

5.3.4.4 Ranking Identified Flows

We model the rank value κ assignment given vector of region of cumulative incremental change computed as:

$$\bar{\alpha}_i^{d_i} \quad (21)$$

For m number of flows contributing traffic δ . We compute rank as:

$$\kappa_{u,v} = \sum \frac{\delta(u, v) - \delta'(u, v)}{\max(\delta(u, v), \delta'(u, v))} \quad (22)$$

Where δ and δ' are weights contribution at t and t' . Equation (22) ranks each candidate flow based on the change in traffic and amount of traffic load contribution. Notice that the rank of a flow increases with normalized value $\delta(u, v) - \delta'(u, v) > 0$ and reduces with $\delta(u, v) - \delta'(u, v) < 0$. This way only the flows with consistent high traffic load contribution are chosen.

5.4 Throughput Simulation Results & Discussion

To demonstrate the strength of our proposed strategy, using scenario 3 described above, we have created a scalable network simulation environment written in java with optical and wireless

components adapted and modified from SSFnet scalable simulator. The traffic for popularity of accessing particular broadband service is generated using Bimodal Zipf; session arrivals using exponential for short time-scales, time-of-day and time-zone using correlated behaviour; and finally session durations using heavy-tailed" distributions. Figure 42 shows the configuration delays experienced when ARN based traffic engineering (AN-TE) is implemented and without such capabilities (AN-NTE). The result shows up to 60% reduction in average configuration delay at a data transfer size of 1 GB, where it can be seen that the delay per MB of data (at a data request of 1 GB) is reduced from 1.7 s (light grey circles) down to 0.7 s (dark grey crosses).

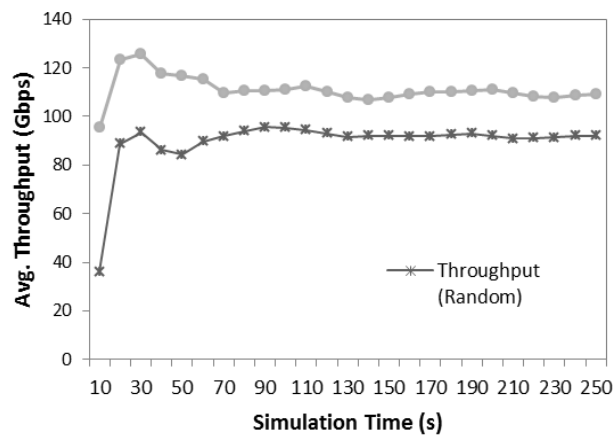


Figure 42: Result showing the effect of flow selection techniques on throughput.

We attribute this improvement to the suitability of the chosen traffic for switching in the high priority link. Figure 43 shows the throughputs attained by both the AN-TE and AN-NTE models, with the AN-NTE (i.e. non traffic-engineered) solution serving as a baseline comparison. AN-TE improves the throughput by 40% at simulation time 40s, where the throughput is increased from 82 MB/s for the AN-NTE case (red circles) up to 115 MB/s for the AN-TE situation. Over a longer time period, where there is a steady-state situation, we can see that the flow-selection approach offers an average improvement 22% over all AN-NTE throughput values, rising from an average of 92 MB/s for the AN-NTE flow up to an average 110 MB/s for the AN-TE traffic-engineered flow.

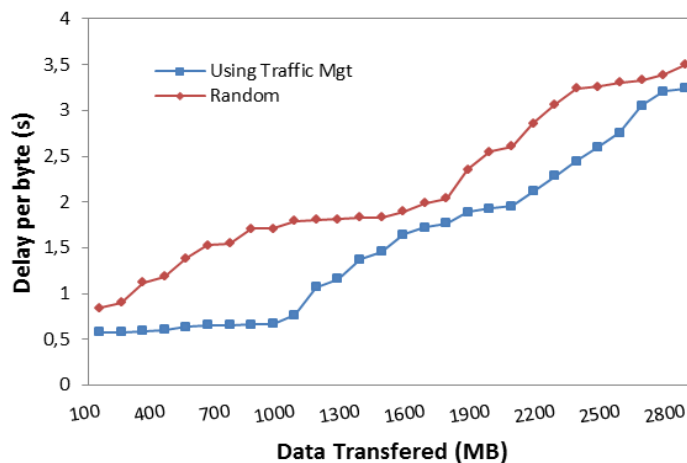


Figure 43: Comparing the effectiveness of adopting a connectivity traffic measure with simple random assignment. Configuration delay is measured in seconds (s)

Future work will be directed towards simulating the other two scenarios outlined earlier, to better understand the relative performance of these situations when flow scheduling traffic management is used, so as to provide better indications for the relative allocations onto the high and low priority wavelengths.

6 Conclusions

In this deliverable D1.2 “ARN Modeling” of the SODALES project we have provided a comprehensive overview of the research technologies, methodologies and modeling results that we have undertaken to better understand the design specifications for the ARN architecture. We have provided a study of the competing electro-optic and all-optical technologies that could provide the required advanced functionalities of the SODALES ARN, although in order to fabricate the final demonstrator using commercial-off-the-shelf components, and from the perspective of reliability, maintenance and robustness, and avoiding potential technical roadblocks in the project, we are expecting the final ARN demonstrator to consist of an electrical technical solution.

We have described some of the RF (60GHz) and optical final-drop technologies that will enable the wireless interfacing between ARN and end-users, with some experimental results for the high capacity line-of-sight (LoS) optical solutions.

With energy efficiency becoming an ever more critical aspect of modern telecommunications, we have also described our methodology and the theory underpinning our novel analysis of the fundamental limits of absolute energy efficiency in a converged (wireless (RF) and fixed-line optical fibre) communications system. Our theory will find application in providing a tool for the competitive analysis of a generic range of telecoms technologies, each possessing different noise properties. We have also briefly described some of the renewable powering approaches that could provide remote and independent energy to a stand-alone ARN architecture. Apart from lowering overall carbon footprint, such independent powering can also increase ARN reliability and reduce powering outage possibilities.

We have also provided a detailed service quality analysis, for a novel flow scheduler approach to optimizing the traffic bandwidth management at the ARN over two (low and high priority) wavelengths connecting the ARN to the CO for differentiated service provisioning for the various types of end-users. We have simulated the improvement in data-capacity throughput (by up to 40%) and the reduced latency (by up to 60%) when our ARN-based traffic management system is employed. The simulation modeling is assisting in optimizing the various statistical multiplexing ratios that are evident within the ARN, and the offloading decision thresholds for the varying priority wavelengths.

This deliverable D1.2 has been written in conjunction with the parallel deliverable D1.3, which describes the OAM and control plane building blocks. Particularly for the ARN traffic management results described in this deliverable D1.2, the associated control plane implications can be accessed in the accompanying D1.3 SODALES deliverable.

In the short term, the results described in this deliverable will be fed into the final deliverable D1.4 of the workpackage 1, which provides an overall simulation of the SODALES architecture, and will be completed at the end of Month 18 of the project. In addition, the research described in this deliverable D1.2 will also feed into the workpackage 2, and the task T2.1, which defines the ARN switching fabric design and interfacing. Longer term into the project, the design of the ARN prototypes in the workpackage 4, particular the demonstrator concept of task T4.1 will also be informed by the results flowing from this deliverable D1.2.

7 References

- [1] B. Ramamurthy and B. Mukherjee, "Wavelength conversion in WDM networking," Selected Areas in Communications, IEEE Journal on, vol. 16, pp. 1061-1073, 1998.
- [2] Y. Ni, J. Hyun-Do, I. T. Monroy, H. de Waardt, and T. Koonen, "All-Optical Multi-Wavelength Conversion with Negative Power Penalty by a Commercial SOA-MZI for WDM Wavelength Multicast," in Optical Fiber Communication and the National Fiber Optic Engineers Conference, 2007. OFC/NFOEC 2007. Conference on, 2007, pp. 1-3.
- [3] C. Stamatiadis, K. Vrysokinos, L. Stampoulidis, A. Maziotis, Z. Sheng, D. Van Thourhout, et al., "All-optical wavelength conversion at 160Gb/s using an SOA and a 3rd order SOI nanowire periodic filter," in IEEE Photonics Society, 2010 23rd Annual Meeting of the, 2010, pp. 268-269.
- [4] Y. Lianshan, A. E. Willner, W. Xiaoxia, Y. Anlin, A. Bogoni, Z. Y. Chen, et al., "All-Optical Signal Processing for UltraHigh Speed Optical Systems and Networks," Lightwave Technology, Journal of, vol. 30, pp. 3760-3770, 2012.
- [5] K. Igarashi and K. Kikuchi, "Optical Signal Processing by Phase Modulation and Subsequent Spectral Filtering Aiming at Applications to Ultrafast Optical Communication Systems," Selected Topics in Quantum Electronics, IEEE Journal of, vol. 14, pp. 551-565, 2008.
- [6] A. E. Willner, O. F. Yilmaz, W. Jian, W. Xiaoxia, A. Bogoni, Z. Lin, et al., "Optically Efficient Nonlinear Signal Processing," Selected Topics in Quantum Electronics, IEEE Journal of, vol. 17, pp. 320-332, 2011.
- [7] I. Ashry and H. M. H. Shalaby, "All-optical variable delay buffer for next generation optical networks," in Transparent Optical Networks (ICTON), 2010 12th International Conference on, 2010, pp. 1-3.
- [8] G. Berrettini, G. Meloni, F. Scotti, L. Poti, and A. Bogoni, "Variable all-optical buffering for DQPSK packets," in Optical Fiber Communication Conference and Exposition (OFC/NFOEC), 2012 and the National Fiber Optic Engineers Conference, 2012, pp. 1-3.
- [9] G. Berrettini, G. Meloni, L. Poti, and A. Bogoni, "All-Optical Variable Buffer Based on Semiconductor Optical Amplifier," Quantum Electronics, IEEE Journal of, vol. 47, pp. 510-516, 2011.
- [10] M. Dzanko, B. Mikac, and V. Miletic, "Availability of all-optical switching fabrics used in optical cross-connects," in MIPRO, 2012 Proceedings of the 35th International Convention, 2012, pp. 568-572.
- [11] C. Porzi, G. Meloni, M. Secondini, L. Poti, G. Contestabile, and A. Bogoni, "All-Optical Switching of QPSK Signals for 100 G Coherent Systems," Lightwave Technology, Journal of, vol. 30, pp. 3010-3016, 2012.
- [12] C. Porzi, G. Contestabile, and A. Bogoni, "All-optical simultaneous drop and wavelength conversion of DPSK data," Opt. Lett., vol. 37, pp. 2523-2525, 07/01 2012.
- [13] W.-C. Yan, Z.-Y. Guo, N. Zhu, and Y.-Q. Jiang, "Proposal of a wavelength filter with a cut corner based on Equilateral-Triangle-Resonator," Opt. Express, vol. 21, pp. 16536-16540, 07/15 2013.
- [14] Y. Wakayama, A. Okamoto, A. Tomita, H. Nihei, S. Honma, and K. Suzuki, "Improvement of diffraction efficiency for all-optical tunable wavelength filter by apodized photorefractive grating," in Optoelectronics and Communications Conference (OECC), 2010 15th, 2010, pp. 692-693.
- [15] J. L. Wei, E. Hugues-Salas, C. Sanchez, X. Q. Jin, R. P. Giddings, I. Pierce, et al., "Improved power budgets of end-to-end real-time optical OFDM PON systems using wavelength-offset

- optical filtering," in Communication Systems, Networks & Digital Signal Processing (CSNDSP), 2012 8th International Symposium on, 2012, pp. 1-3.
- [16] A. L. Yi, L. S. Yan, B. Luo, W. Pan, and J. Ye, "All-Optical Signal Regeneration in Polarization-Division-Multiplexing Systems," Photonics Journal, IEEE, vol. 3, pp. 703-712, 2011.
 - [17] G. Contestabile, "All-optical signal regeneration using SOAs," in Communications and Photonics Conference and Exhibition (ACP), 2010 Asia, 2010, pp. 7-8.
 - [18] E. Shiraki, N. Nishizawa, and K. Itoh, "All-optical signal regeneration using pulse trapping in birefringent fibers," in Lasers and Electro-Optics (CLEO) and Quantum Electronics and Laser Science Conference (QELS), 2010 Conference on, 2010, pp. 1-2.
 - [19] J. Wang, H. Ji, H. Hu, H. C. H. Mulvad, M. Galili, E. Palushani, et al., "All-optical 2R regeneration of a 160-Gbit/s RZOOK serial data signal using a FOPA," in Photonics Conference (IPC), 2012 IEEE, 2012, pp. 108-109.
 - [20] Z. Yueying, Z. Min, L. Mintao, L. Lei, and C. Xue, "All-optical QPSK signal regeneration based on XPM in semiconductor optical amplifier," in Communications and Photonics Conference (ACP), 2012 Asia, 2012, pp. 1-3.
 - [21] D. Raychaudhuri et al., "Frontiers of Wireless and Mobile Communications" Proc. IEEE Volume: 100, Issue: 4, pp. 824 – 840, April 2012.
 - [22] S. Koenig et al., "100 Gbit/s Wireless Link with mm-Wave Photonics", OFC 2013, PDP5.B.4, Anaheim, Los Angeles, March 2013
 - [23] A.A.B Raj, et al., "Terrestrial free space line of sight optical communication (TFSLSOC) using adaptive control steering system with laser beam Tracking, Aligning and Positioning (ATP)", Chennai, India, January 2010.
 - [24] info.fsona.com
 - [25] N. Agawal et al., "Design of free space optical omnidirectional transceivers for indoor applications using non-imaging optical devices", Proc. SPIE 7091, Free-Space Laser Communications VIII, August 2008.
 - [26] Recommendation ITU-R P.676-9 (02/2012). Attenuation by atmospheric gases.
 - [27] <http://www.bridgewave.com>
 - [28] <http://www.ubnt.com>
 - [29] EU Commission Decision 2005/50/E
 - [30] NEC Sets Out Vision for Wireless Backhaul of Small Cells, NEC release, <http://www.nec.co.jp/press/en/1202/1603.html>
 - [31] J. Hansryd and J. Edstam, "Microwave Capacity Evolution," Ericsson Review, vol. 1, 2011
 - [32] P.F. Driessens, G.J. Foschini, "On the capacity formula for multiple input-multiple output wireless channels: a geometric interpretation," IEEE International Conference on Communications (ICC), vol.3, pp.1603-1607.
 - [33] P. Kyritsi, "MIMO capacity in free space and above perfect ground: Theory and experimental results," IEEE Symposium on Personal, Indoor, and Mobile Radio Commun., vol.1, pp. 182-186, Sep. 2002.
 - [34] T. Haustein, U. Kruger, "Smart geometrical antenna design exploiting the LOS component to enhance a MIMO System based on Rayleigh-fading in indoor scenarios," Proc. 14th IEEE Proceedings on Personal, Indoor and Mobile Radio Communications (PIMRC) vol.2, pp.1144-11487-10 Sept. 2003.
 - [35] P. Larsson, "Lattice array receiver and sender for spatially orthonormal MIMO communication", IEEE 61st Vehicular Technology Conference (VTC-Spring), vol.1, 192-196, May 30-June 1, 2005.

- [36] F. Bohagen, P. Orten, G. E. Oien, "Construction and capacity analysis of high-rank line-of-sight MIMO channels," Proc. IEEE Wireless Communications and Networking Conference, 2005, vol.1, pp. 432-437, March 13-17, 2005.
- [37] C. Sheldon, S. Munkyo, E. Torkildson, M. Rodwell, U. Madhow, "Four-channel spatial multiplexing over a millimeter-wave line-of-sight link," Proc. IEEE MTT-S International Microwave Symposium, pp.389-392, 7-12 June 2009.
- [38] J. Hansryd and J. Edstam, "Microwave Capacity Evolution," Ericsson Review, vol. 1, 2011.
- [39] C. Zhou, X. Chen, X. Zhang, S. Zhou, M. Zhao, J. Wang „Antenna Array Design for LOS-MIMO and Gigabit Ethernet Switch-Based Gbps Radio System”, International Journal of Antennas and Propagation, Hindawi, Vol. 2012, Article ID 920624, 10 pages.
- [40] <http://www.gotmic.se/>
- [41] J.R.Makri et al., "Next generation millimeter wave backhaul radio: Overall system design for GbE 60 GHz PtP wireless radio of high CMOS integration" 18th IEEE International Conference on Electronics, Circuits and Systems (ICECS), Dec. 2011.
- [42] Tech. Rep. v1.1.1, July 2009 "Reconfigurable Radio Systems (RRS); Functional Architecture for the Management and Control of Reconfigurable Radio Systems".
- [43] Volker Jungnickel et al. "1 Gbit/s MIMO-OFDM transmission experiments", IEEE VTC Fall 2005.
- [44] W. Keusgen et al. "An NLOS-capable 60 GHz MIMO demonstrator: System concept & performance," IEEE 9th International New Circuits and Systems Conference (NEWCAS) pp.265-268, 26-29 June 2011.
- [45] T.Wirth et al. "Realtime Multi-User Multi-Antenna Downlink Measurements" IEEE Wireless Communications and Networking Conference (WCNC) 2008, pp. 1328-1333, March 2008.
- [46] D. Klaus, editor. Technologies for the Wireless Future, vol. 3. John Wiley & Sons, Ltd., 2008.
- [47] ETSI Technical Committee for RRSs. \TR 102-683: Reconfigurable Radio Systems (RRS); Cognitive Pilot Channel (CPC)." Tech. Rep. v1.1.1, September 2009.
- [48] Liane Grobe, Anagnostis Paraskevopoulos, Jonas Hilt, Dominic Schulz, Friedrich Lassak, Florian Hartlieb, Christoph Kottke, Volker Jungnickel, and Klaus-Dieter Langer, High-Speed Visible Light Communication Systems, accepted for publication in IEEE Communications Magazine, Special Issue on Visible Light Communications, December 2013.
- [49] J. Grubor, V. Jungnickel, and K.-D. Langer, "Adaptive Optical Wireless OFDM System with Controlled Asymmetric Clipping," in 41st Asilomar Conference on Signals, Systems and Computers (ACSSC), 2007, pp. 1896-1902.
- [50] C. Kottke, K. Habel, L. Grobe, J. Hilt, L. Fernández, A. Paraskevopoulos, and K.-D. Langer, "Single-channel Wireless Transmission at 806 Mbit/s using a White-light LED and a PIN-based Receiver," in 14th International Conference on Transparent Optical Networks (ICTON), 2012, invited paper We.B4.1.
- [51] K.-D. Langer, J. Vučić, C. Kottke, L. Fernández, K. Habel, A. Paraskevopoulos, M. Wendl and V. Markov, "Exploring the Potentials of Optical-Wireless Communication using White LEDs," in 13th International Conference on Transparent Optical Networks (ICTON), 2011, invited paper Tu.D5.2.
- [52] C. Lange, D. Kosiankowski, C. Gerlach, F. Westphal, and A. Gladisch, "Energy Consumption of Telecommunication Networks," Paper 5.5.3, ECOC 2010, Vienna, Austria, 2009.
- [53] A. Jirattigalachote, C. Cavdar, P. Monti, L. Wosinska, A. Tzanakaki, "Dynamic provisioning strategies for energy efficient WDM networks with dedicated path protection", Optical Switching and Networking, 8(3), p.201-213, 2011
- [54] H.T. Mouftah, B. Kantarci, "Energy-efficient cloud computing—A green migration of traditional IT', Handbook of Green Communications, p.295-329, 2012

- [55] W. Van Heddeghem, F. Idzikowski, W. Vereecken, D. Colle, M. Pickavet and P. Demeester, "Power consumption modeling in optical multilayer networks", Photonic Network Communications, 2012
- [56] G. Shen, R.S. Tucker, "Energy-minimized design for IP over WDM networks", JOCN, 1(1), p176, 2009
- [57] A. Gladisch, C. Lange, R. Leppia, "Power efficiency of optical versus electronic access networks", European Conference on Optical Communications (ECOC'08), Paper Tu4A2, Brussels, 2008.
- [58] M.C. Parker, S.D. Walker, 'Information transfer and Landauer's principle', Optics Communications, Vol. 229, pp23-27, 2004.
- [59] M.C. Parker, S.D. Walker, 'Differential temperature Carnot heat analysis shows that computing machines are thermodynamically irreversible', Optics Communications, 281, p3440-3446, 2008
- [60] S.J. Ben Yoo, "Energy Efficiency in the Future Internet the Role of Optical Packet Switching and Optical Label Switching", IEEE J. of Selected Topics in Quantum Electronics, 17 (2), p406-418, 2011.
- [61] M.C. Parker, S.D. Walker, 'Roadmapping ICT: An Absolute Energy Efficiency Metric ', JOCN, 3(8), A49 (2011)
- [62] W. Van Heddeghem, M. De Groote, W. Vereecken, D. Colle, M. Pickavet, and P. Demeester, "Energy-Efficiency in Telecommunications Networks: Link-by-Link versus End-to-End Grooming", ONDM 2010, Kyoto, Japan, 2010.
- [63] N. Gershenfeld, "The physics of information technology", Chapter 13, Cambridge University Press, 2000.
- [64] C.E. Shannon, "Communication in the Presence of Noise", Proc. Institute of Radio Engineers, 37 (1), p.10–21, 1949
- [65] M.C. Parker, S.D. Walker, 'Is computation reversible?', Optics Communications, 271, p274-277, 2007
- [66] C. Bock, S. Figuerola, M.C. Parker, T. Quinlan, S.D. Walker, "Convergent radio and fibre access architectures using low-energy systems", ICTON'12, Warwick, UK, June 2012
- [67] L. Brillouin, "Science and Information Theory", 2nd Edition, Academic Press, 1962
- [68] M.C. Parker, S.D. Walker, 'A Dynamic Model of Information and Entropy', Entropy, vol.12(1), p80-88, 2010
- [69] S. Wei-Tao, W. Shing-Wa, C. Ning, and L. G. Kazovsky, "MARIN Hybrid Optical-Wireless Access Network," in Optical Fiber Communication and the National Fiber Optic Engineers Conference, 2007. OFC/NFOEC 2007. Conference on, 2007, pp. 1-3.
- [70] S. Horia, "Residential Area Service Platforms: Modelling Challenges for Multiple Data Traffic Patterns in Wireless Mesh Networks," 2009, pp. 340-345.
- [71] P. Chowdhury, M. Tornatore, S. Sarkar, and B. Mukherjee, "Building a Green Wireless-Optical Broadband Access Network (WOBAN)," Lightwave Technology, Journal of, vol. 28, pp. 2219-2229, 2010.
- [72] C. Ranaweera, E. Wong, C. Lim, and A. Nirmalathas, "Next generation optical-wireless converged network architectures," Network, IEEE, vol. 26, pp. 22-27, 2012.
- [73] C. A. Chan, M. Attygalle, and A. Nirmalathas, "Active remote node with layer two forwarding for improving performance of EPON," in Global Telecommunications Conference, 2008. IEEE GLOBECOM 2008. IEEE, 2008, pp. 1-5.
- [74] L. Kazovsky, S.-W. Wong, T. Ayhan, K. M. Albeyoglu, M. R. Ribeiro, and A. Shastri, "Hybrid optical-wireless access networks," Proceedings of the IEEE, vol. 100, pp. 1197-1225, 2012.

- [75] G. Maier, A. Feldmann, V. Paxson, and M. Allman, "On dominant characteristics of residential broadband internet traffic," in Proceedings of the 9th ACM SIGCOMM conference on Internet measurement conference, 2009, pp. 90-102.
- [76] W.-T. Shaw, Hybrid Optical Wireless Access Networks: ProQuest, 2009.
- [77] L. Yan, W. Jianping, Q. Chunming, A. Gumaste, X. Yun, and X. Yinlong, "Integrated Fiber-Wireless (FiWi) Access Networks Supporting Inter-ONU Communications," Lightwave Technology, Journal of, vol. 28, pp. 714-724, 2010.
- [78] Q. Zhao and C.-K. Chan, "A wavelength-division-multiplexed passive optical network with flexible optical network unit internetworking capability," Lightwave Technology, Journal of, vol. 25, pp. 1970-1977, 2007.
- [79] S. Pato, J. Pedro, J. Santos, A. Arsénio, P. Inácio, and P. Monteiro, "On Building a Distributed Antenna System with Joint Signal Processing for Next Generation Wireless Access Networks: The FUTON Approach," in 7th Conference on Telecommunications, Portugal, 2008.
- [80] I. 802.16-2009, "IEEE Standard for Local and metropolitan area networks," 2009.
- [81] C. Baugh, J. Huang, R. Schwartz, and D. Trinkwon, "Traffic model for 802.16 TG3 MAC/PHY simulations," IEEE, vol. 802, pp. 2002-2005, 2001.
- [82] K. Sripanidkulchai, B. Maggs, and H. Zhang, "An analysis of live streaming workloads on the internet," presented at the Proceedings of the 4th ACM SIGCOMM conference on Internet measurement, Taormina, Sicily, Italy, 2004.
- [83] N. McKeown, T. Anderson, H. Balakrishnan, G. Parulkar, L. Peterson, J. Rexford, S. Shenker, and J. Turner, "Openflow: enabling innovation in campus networks," SIGCOMM Comput. Commun. Rev., vol. 38, pp. 69–74, March 2008.
- [84] F. S. H. Joshua A. Taylor, "Laplacians for flow networks," MIT, 2011.
- [85] H. Bunke, "A graph-theoretic approach to enterprise network dynamics," 2007.[Online]. Available: <http://ebooks.ulb.tu-darmstadt.de/11220/>.
- [86] D. U. Xavier Bresson, Thomas Laurenty and J. H. von Brecht, "Convergence and energy landscape for cheeger cut clustering," in In NIPS, pp. 1394-1402, 2012.
- [87] S. Sarkar and K. Boyer, "Quantitative measures of change based on feature organization: eigenvalues and eigenvectors," in Computer Vision and Pattern Recognition, 1996. Proceedings CVPR '96, 1996 IEEE Computer Society Conference on, jun 1996, pp. 478 –483.
- [88] S. Sarkar and K. L. Boyer, "Quantitative measures of change based on feature organization: Eigenvalues and eigenvectors," in Computer Vision and Pattern Recognition, 1996. Proceedings CVPR'96, 1996 IEEE Computer Society Conference on. IEEE, 1996, pp. 478–483.